Investigation of Ducts as a "Radar Pinhole" for Detecting Objects Through a Wall

by

Nicholas John Whitelonis, B.S.E.E.

Thesis

Presented to the Faculty of the Graduate School of

The University of Texas at Austin

in Partial Fulfillment

of the Requirements

for the Degree of

Master of Science in Engineering

The University of Texas at Austin

August 2009

The Thesis Committee for Nicholas John Whitelonis certifies that this is the approved version of the following thesis:

Investigation of Ducts as a "Radar Pinhole" for Detecting Objects Through a Wall

Approved by
Supervising Committee:

_____

Hao Ling, Supervisor

_____

Andrea Alu

Acknowledgements

I would like to acknowledge my supervising professor, Dr. Hao Ling, for providing support and guidance throughout my research and academic pursuits. I would also like to thank Dr. Ling for providing his invaluable experience and knowledge that has helped strengthen my understanding of the subject matter and has greatly increased the caliber of this thesis.

I would like to extend my thanks to Dr. Andrea Alu for agreeing to serve as a reader for this thesis and for offering encouragement on the work done for this thesis.

I would also like to thank Andrew Valdez for providing measurement support during the through wall experiments.

Abstract

Investigation of Ducts as a "Radar Pinhole" for Detecting Objects Through a Wall

Nicholas John Whitelonis, M.S.E.

The University of Texas at Austin, 2009

Supervisor: Hao Ling

There is a continuing interest in the through-the-wall capabilities of radar. It has been found that walls behave as a low-pass medium, and therefore through-the-wall radar has been restricted to frequencies in the low GHz range. Unfortunately at these lower frequencies the resolution of the radar system is sacrificed. This thesis investigates the possibility of using a duct as a means of detecting objects through a wall.

Ducts have been extensively studied in the past; however there has been limited research of ducts with two open ends. In this thesis the difference between an open-ended duct and a duct with two open ends is investigated through measurement and simulation. For simulation an approximate method is used that treats the duct as a waveguide. It is found that a significant amount of power is transmitted through a duct with two open ends. It is then shown that an object can be detected through a wall by using a duct that has been inserted into the wall. Then the two-way insertion loss of a duct with two open

ends is determined through measurement and simulation. It is shown that a duct behaves as a high-pass medium and can be used as a propagation channel through a wall. The insertion loss due to the duct and the insertion loss through a concrete wall are compared

Table of Contents

List of Tables

List of Figures

x

Chapter I: Introduction

There has been an ongoing interest in the through-the-wall capabilities of radar for use in military applications, security and surveillance, and search and rescue [1-3]. Research done on the topic of through-the-wall radar has focused on characterizing the transmission properties of different walls and on developing different systems for through wall observation [4-7]. The possibility of using ultra-wideband systems has been investigated as well as the capabilities of continuous-wave (CW) Doppler systems. Walls can be quite lossy and highly dispersive, thus introducing many artifacts to the acquired radar data. Significant efforts have been devoted to characterize wall effects and in finding methods to remove wall effects [8-12]. More recently, there is also an emerging interest in exploiting the infrastructure of a building as a means of gaining better awareness of the building's interior [3]. Ducts are a common structure found in a building, such as a drainage pipe, an air conditioning duct, or a hole in the wall itself. The goal of this thesis is to investigate the possibility of using a duct as a propagation channel for gaining information about a building's interior. Therefore it is important to understand the propagation and scattering mechanisms of a duct that has an opening at both ends.

Motivated by the study of scattering from jet engine intakes, there have been extensive studies of open-ended ducts, which for the purpose of this thesis refer to ducts that are open on one end and have a conducting termination on the other end. Surprisingly, there is very limited information from the literature on ducts with two open ends. As early as 1968 a semi-infinite circular duct was used to model the intake of a jet engine [13]. An open-ended circular duct was used because the geometry is simple and an exact closed-form solution for the back scatter could be obtained using the Wiener-

1

Hopf technique, as derived and presented by Bowman [14]. The limitation of the exact solution was that the final result was too complex to be useful given the numerical capabilities at the time. Chuang, Liang, and Lee later derived an asymptotic approximate of the Wiener-Hopf solution valid at high frequencies [15]. In the asymptotic expansion only the first and second order terms are considered, which reduces the numerical burden of the solution. In 1982 Johnson and Moffatt compared the approximate solutions of Wiener-Hopf to exact numerical computations [16]. In the same year, Medgyesi-Mitschang and Eftimiu solved a finite circular duct using the method of moments (MoM) with a body of revolution basis for modeling the duct [17]. In 1983 Huang introduced a method for solving the backscatter from a circular duct by expanding the incident field in terms of the modes for a circular waveguide [18]. The modal expansion method based on Huang's work could be applied to any duct that behaved as a waveguide and maintained a constant cross-section. Burkholder, Chuang, and Pathak used a hybrid modal method and moment method technique to compute the backscatter from tapered ducts in 1988 [19]. Later, Burkholder used a hybrid mode-asymptotic technique to solve for the backscatter from waveguide ducts with bends [20]. Boonzaaier and Malherbe came up with a model for the termination at the backend of a duct that better represented what would be found in a jet engine intake [21].

In the late 1980's, advances in computational methods for approximating the backscatter from ducts allowed researchers to analyze structures other than waveguide type structures. In 1989 a new technique to compute the radar cross-section (RCS) from a duct or cavity was presented by Ling, Chou, and Lee [22]. The technique referred to as shooting and bouncing rays (SBR), uses ray tracing to account for multiple bounces inside the duct structures and then applies physical optics on the rays exiting the duct to compute the backscatter. The SBR technique was useful for high-frequency scattering

2

and arbitrary cavities and ducts, but deviated from experimental results at low frequencies where modal methods had been successful in the past [23]. The generalized ray expansion (GRE) method was subsequently proposed to improve the accuracy of SBR [24]. The work done in the late 1980's allowed for high fidelity modeling of intakes on different aircraft.

A different track of research on ducts focused on understanding the complex scattering phenomenology found in these concave structures. In 1993 Moghaddar and Walton used joint time-frequency distributions to analyze the backscatter from an open-ended circular duct [25]. Using the short-time Fourier transform (STFT) and the Wigner-Ville distribution, they demonstrated that the scattering features from a waveguide type structure became very revealing in the joint time-frequency space. The various mechanism associated with the modes in the waveguide could be easily identified and interpreted. It was also shown that the STFT was superior for backscatter analysis because Wigner-Ville distributions have cross-terms that represent false features. Kim and Ling showed that wavelets could be used to analyze the scattering mechanisms of open-ended circular ducts [26]. Most recently in 2007 Ling and Ram applied the reassigned joint time-frequency transform to an open-ended circular duct [27].

Despite the extensive publications on the backscatter from cavities and ducts there is very little information about circular ducts that have two open ends. Medgyesi-Mitschang solved a duct with two open ends using MoM [28]. However the duct was electrically small and the solution was done for the purpose of code validation. A duct with two open ends was not investigated in previous works because the two open ends would not accurately portray a jet engine intake.

The first objective of this thesis is to study the backscatter from a duct with two open ends through measurement and simulation. The results will focus on differences to

3

the well understood open-ended circular cylinder. The second objective of this thesis is to investigate whether a target can be seen through a wall using a duct as a "radar pinhole" into the room.

The remainder of the thesis is organized into three chapters. Chapter II discusses the design of a test-site for making RCS measurements. A suitable measurement methodology is presented followed by an explanation of the design decisions made when building a test-site and how they influence the quality of measurements. Measurements made on the range are then validated against simulation for a sphere. Chapter III focuses on the scattering from a hollow circular duct. A comparison is made between an open-ended duct and a duct with two open ends through measurement and simulation. A review of the finite open-ended circular duct is first presented as well as a modal method for simulation based on Huang's formulation [18]. Having reviewed the open-ended duct, the circular duct with two open ends is measured for comparison. The modal method is then modified to take into account the second open end. In the analysis of the duct with two open ends it is found that a significant amount of power is radiated through the backend. Chapter IV then investigates the possibility of using the power radiated from the backend to observe a target through the duct with two open ends. The modal method of simulation is once again modified and compared to measured results. The measured insertion loss of the duct with two open ends is determined and shown to be in agreement with simulation. The chapter finishes with a comparison of the insertion loss due to the duct and the insertion loss through a concrete wall as presented by Gibson and Jenn [8]. The fifth and final chapter draws conclusions from the presented work and outlines future extensions from this work.

Chapter II: Measurement Test-Site Design and Validation

2.1. INTRODUCTION

The purpose of this chapter is to design an appropriate test-site for measuring the Radar Cross-Section (RCS) of an open-ended duct. The second section outlines the process of taking an RCS measurement. The third section discusses the design decisions made when building a test-site and how they apply to the test-site used for measurements in this thesis. The final section presents a validation of the test-site against simulation using a sphere as the target.

2.2. RCS MEASUREMENT METHODOLOGY

For making RCS measurements a vector network analyzer (VNA) was used as the source and receiver. One drawback of using a VNA is that it has a limited power output. Having a limit on the amount of power gives a maximum possible range before the backscatter from the target will drop below the noise-floor.

To measure the RCS accurately, two measurements must be taken with the VNA, one with the target in place and one without the target, which is considered the background. The background data is then subtracted from the target plus background data in order to suppress scattering from clutter in the environment. Background subtraction is very useful for making measurements; however it comes with some limitations. Any interactions between the target and the test environment will not be subtracted, such as ground-bounce. Background subtraction also does not work well when the RCS of the background clutter is substantially higher than the RCS of the target.

When making RCS measurements with a VNA, a common setup is to use two antennas and measurements are taken through S_{21} or S_{12}. It is also possible to use a single antenna and measure S_{11}. When making RCS measurements through S_{21} or S_{11} there is

always some interaction with the antenna that will appear as a feature in the range profile. When measuring through S_{21} there will be a direct feed-through from one antenna to the other, which will appear as a strong scattering feature in the range profile. Background subtraction can successfully suppress the direct feed-through to a level that is below the noise floor. When one antenna is used and measurements are made through S_{11} there will be reflections from the feed port of the antenna. There may be multiple reflections, for example in the case of a horn antenna there will also be reflections from the mouth of the horn. Just as with the direct feed-through, these reflections from the antenna will appear as scattering features in the range profile. Background subtraction will suppress the magnitude of the reflections but will not suppress them to a level that is below the noise floor. Therefore the reflections from the antenna will always be present in the range profile, even after applying background subtraction. Provided the target is sufficiently far from the antenna it will be clear which features in the range profile are from the antenna, and which are from the target. The advantage to measuring through S_{11} instead of S_{21} is that the measurements are guaranteed to be monostatic.

2.3. TEST-SITE DESIGN

Figure 1 shows the test-site used for making backscatter measurements in this thesis. The remainder of this section discusses the design decisions made when building the test-site and how they impact the RCS measurements. The first decision was to determine how far from the target the measuring antennas should be placed. The minimum separation between antennas and target is dependent on the antenna used for measurement and the size of the target. The remainder of the design focuses on reducing the interaction between the target and the test environment.

When making RCS measurements in the lab, it is important to insure that the target is in the far-field of the measuring antenna and that the antenna is in the far-field of the subsequent scattering from the target, that the illuminating waveform is planar, and that the scattering takes place in free-space. There are many factors that lead to deviations from the ideal excitation that must be taken into account in order to make quality measurements. If obstacles cannot be overcome, understanding where inaccuracies are introduced can explain deviations from expected results.

Figure 1 Test-site used for RCS measurements

Test-site design starts at the transmitter and receiver. As discussed in the previous section RCS measurements can be taken using two antennas, one acting as the transmitter and the other as the receiver. By exciting one antenna and measuring the backscatter on the second antenna, the unnormalized RCS will be measured. The first step is to choose an appropriate antenna. Having chosen an antenna, there are three factors that influence

the minimum distance between the target and antenna: the far-field zone of the antenna, the wave front of the antenna, and when making monostatic RCS measurements using two antennas the target has to be far enough away such that it can be assumed that the two antennas are co-located.

Since a planar wave-front is desired, a parabolic reflector antenna would be the obvious choice since it, by design, provides a plane-wave in the near-field zone in addition to the far-field zone. When using other antennas, such as a horn, that have a spherical wave-front then it is necessary to define how far from the antenna the target must be so that the wave-front is nearly planar with respect to the target. The phase taper is defined to be the phase difference between the middle of the target and the greatest extent of the target [29]. The phase taper is a measure of the deviation of the spherical wave front from the ideal plane wave, illustrated in Figure 2. Equation (2.1) is used to calculate the minimum range to the target based on the greatest dimension of the target, D, and the wavelength of operation, λ. The variable k is used to define the phase taper. An acceptable phase taper is given to be 22.5°, which corresponds to $k=2$ [29]. The implication of equation (2.1) is that for an electrically large target, the target has to be placed further from the antenna or else it can no longer be assumed that the excitation is cophasal.

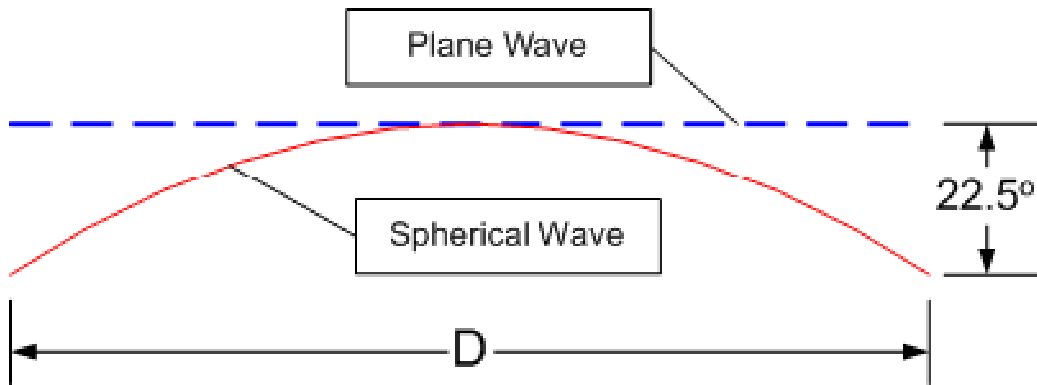$$(2.1) \qquad R_{min} = {k \cdot D^2}/{\lambda}$$

Figure 2 Phase taper

Insuring that the target is in the far-field is dependent on the size of the antenna with respect to wavelength. Equation (2.2) is the well known equation for the far-field zone of the antenna. It resembles equation (2.1), with the difference being that D now corresponds to the dimension of the antenna, and not the target.

$$(2.2) \qquad R_{min} = \frac{2 \cdot D^2}{\lambda}$$

When making monostatic measurements it is necessary to use the same location for transmitting and receiving the radar signal. When using two antennas, one as transmitter and the other as receiver, they can assume to be co-located provided the distance from the antennas to target is significantly greater than the separation between the two antennas. Therefore the antennas need to be placed as close together as possible, which will be a function of their physical shape and size.

RCS is a measure of the reflected power in free-space, therefore it is important to consider what will approximate a free-space environment when the measurement test-site is not in free-space. The ideal situation would be to suspend the target high into the air in an open field. This is not always practical and by making some quick checks free-space can be approximated. When close to the ground, ground-bounce reflections will influence results; therefore it is necessary to use absorbers on the ground to minimize these

9

reflections. When taking measurements indoors the reflections from walls and ceiling should also be acknowledged and suppressed. Removing any potential clutter away from the target is also necessary to make sure there are no interactions between the target and the environment. Surrounding the target with absorbers can help minimize target-environment interactions. The supporting structure for the target must also be chosen so that it will not influence the target's RCS. A support structure with a low RCS is ideal. This can be achieved by using a material such as foam that has a permeability and permittivity close to that of free-space, or by using a structural shape that is designed to have a low RCS.

2.4. TEST-SITE VALIDATION

To validate the measurement setup, the measured results are compared with Method of Moments (MoM) simulation using a sphere. A sphere is an ideal target for validation because it is well understood and there is no risk of misaligning the target with the transmit and receive antennas. For the sphere it is expected that two strong features will be seen in the range profile. The first feature will be from the front of the sphere, labeled 1 in Figure 3, and a second return some time later from a creeping wave traveling around the back of the sphere, labeled 2 in Figure 3. The distance between these two features will be a function of the sphere's radius.
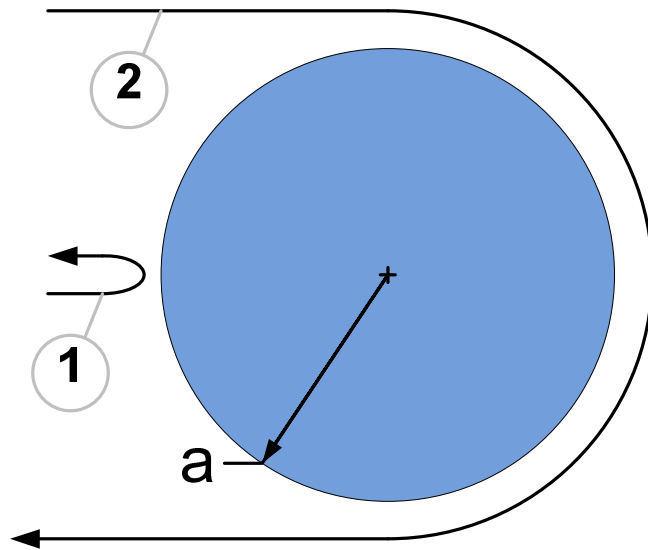
Figure 3 Scattering from a sphere

A Perfect Electric Conductor (PEC) sphere with a radius of 28.5mm was simulated using the MoM solver FEKO. The frequency-domain RCS is shown in Figure 4. The RCS of a racquetball wrapped in aluminum foil, shown in Figure 6, measured using the test-site described previously is shown in Figure 5. When comparing the frequency-domain RCS of the simulated sphere to the measured sphere it is not clear that there is good agreement between measurement and simulation. It is possible to make out the main oscillation due to interference between the main reflection and creeping wave of the sphere which repeats every 2 GHz in both simulation and measurement. Two targets far apart will have a fast oscillation in the frequency-domain, and targets closer together will have a slower oscillation. Therefore it can be concluded that the high-frequency jittering in Figure 5 is either noise in the measurement or interference from background clutter.

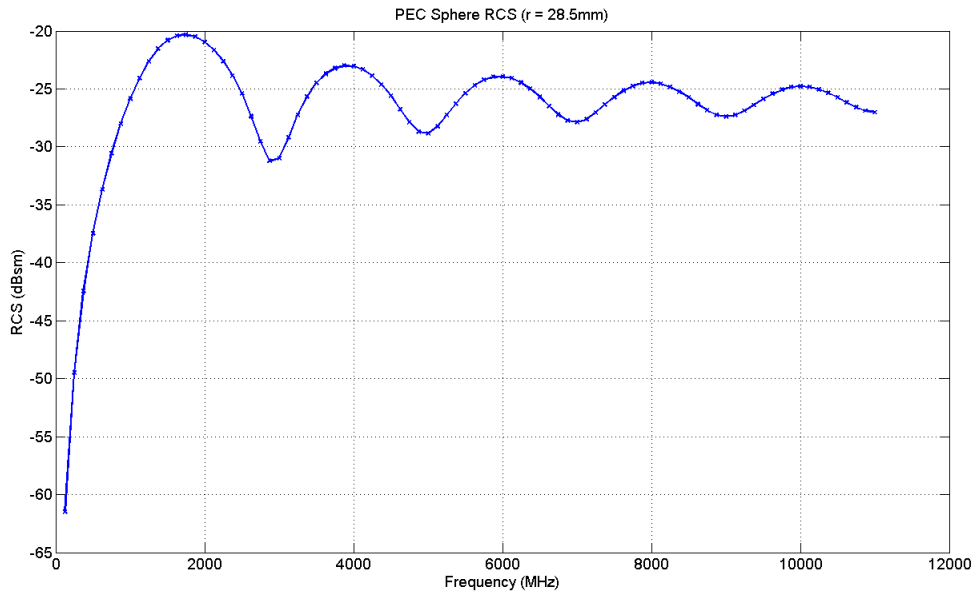Figure 4 Frequency response of PEC sphere simulated using FEKO
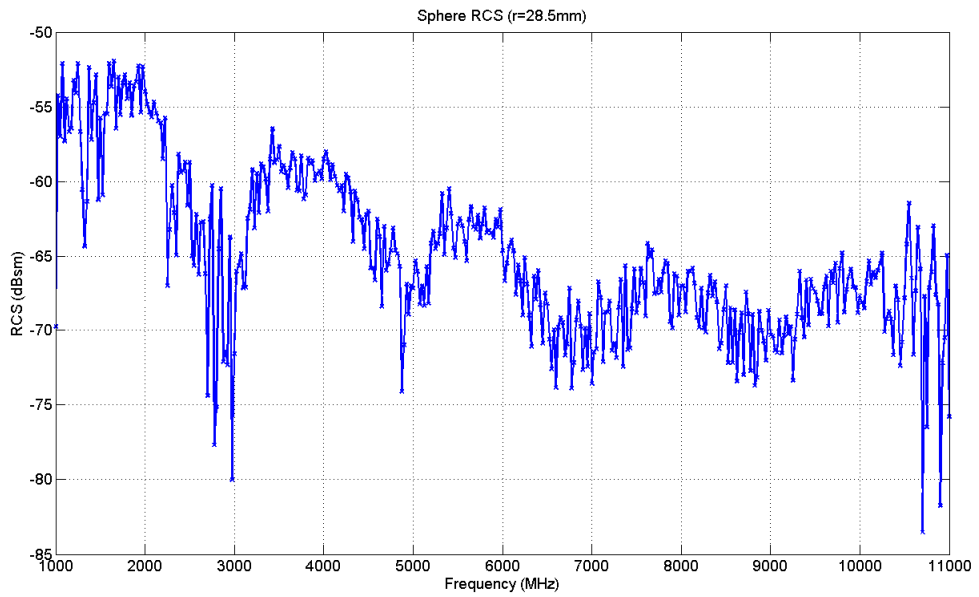
Figure 5 Frequency response of measured sphere
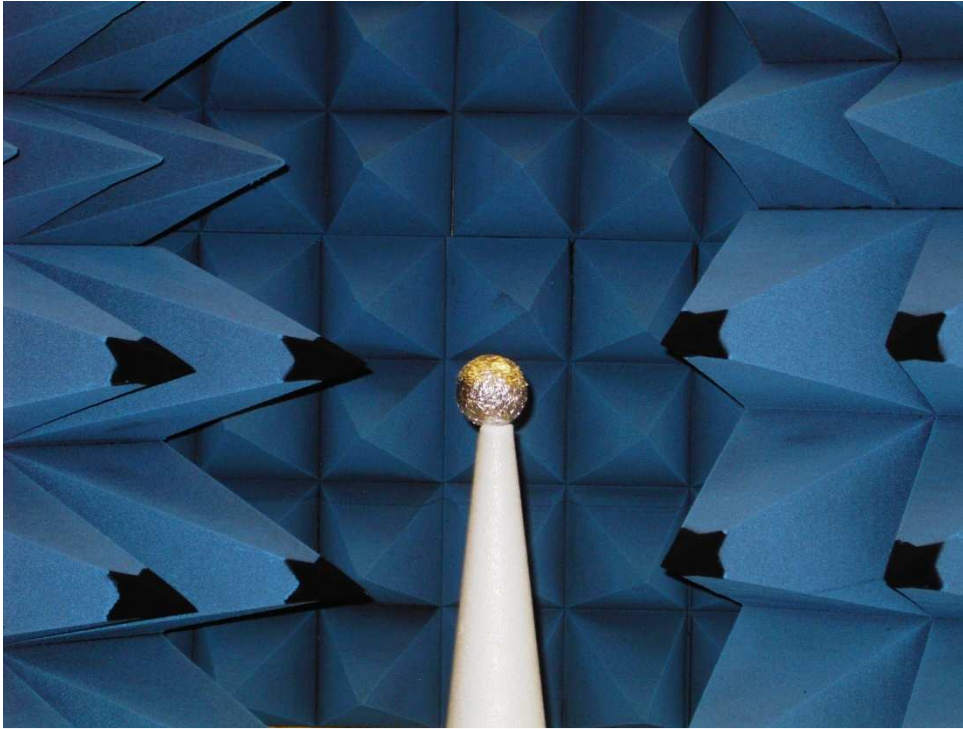
Figure 6 Sphere used for validation of test-site

By applying an inverse Fourier transform to the frequency-domain data, the range profile of the sphere is obtained. In the range profile it is expected that there will be two peaks, one from the head-on reflection and the second from the creeping wave. Based on the geometry of the sphere it is expected that the separation in range between the two peaks will be 73.3mm. For the FEKO simulation, Figure 7, there is a difference of 72.6mm, and the measurement, Figure 8, shows a difference of 80mm. Considering how crude the sphere used for measurement is, especially the roughness of its surface, it can be said that the simulation and measurement agree fairly well. It is important to qualify what is meant when it is said that the measurement and simulation agree well. It is clear that the magnitude of the RCS does not agree and some form of normalization would be required for an agreement of the magnitude of the RCS. For example the gain of the measuring antennas and the path loss are included in the measurement and would need to

13

be taken into account. However, even without such normalization it is still possible to make broadband measurements that accurately portray the scattering features of a target, such as the first bounce and creeping wave from the sphere. Therefore given that the scattering features in simulation agree well with the measured scattering features it is possible to proceed with a degree of confidence in our measurements.
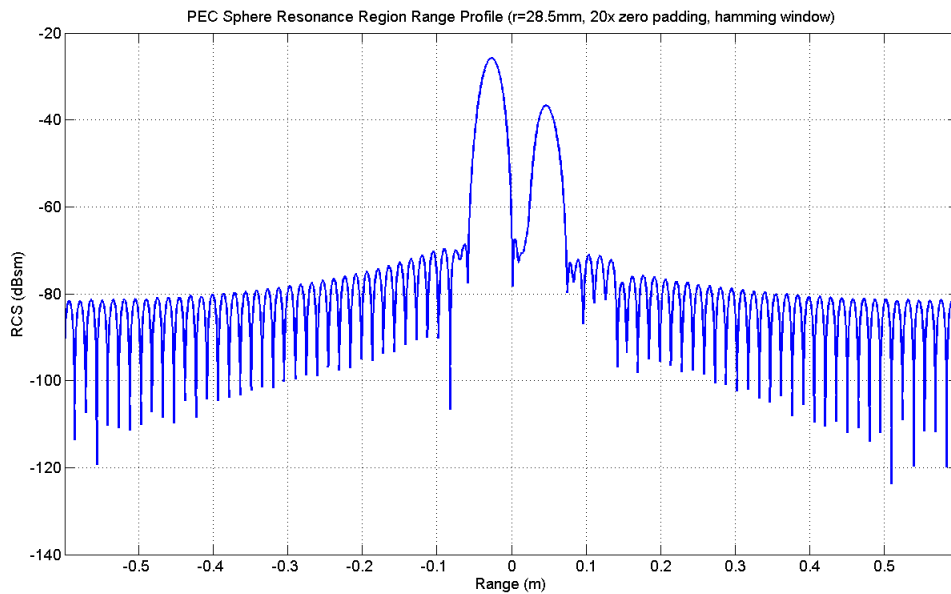

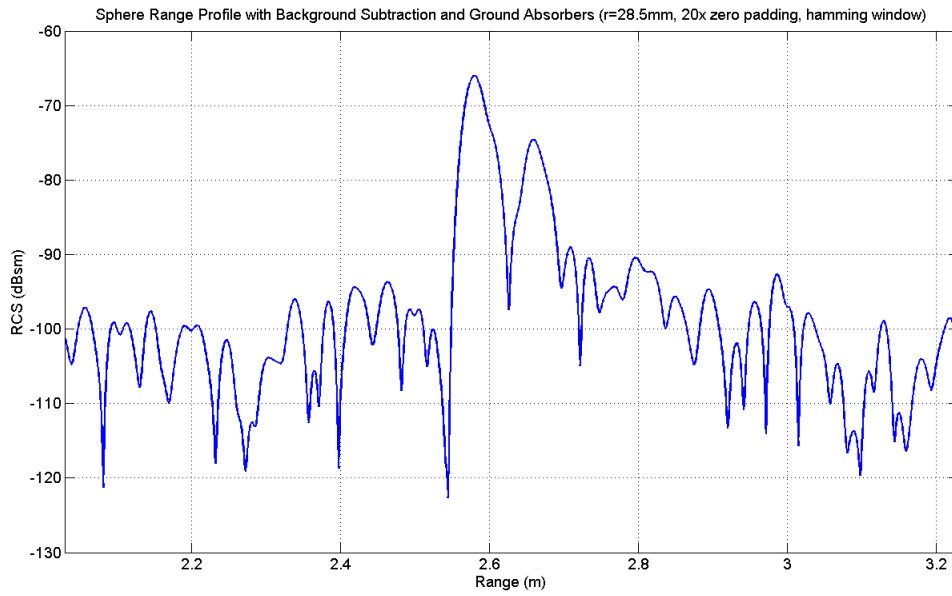Figure 7 Range profile of PEC sphere simulated using FEKO

14

Figure 8 Measured range profile of sphere

Chapter III: Measurement and Simulation of Ducts

3.1. INTRODUCTION

The purpose of this chapter is to compare the difference between an open-ended duct and a duct with two open ends. An open-ended duct refers to a duct with one end open and the other end shorted, where as a duct with two open ends has both ends open. For the purposes of this discussion a hollow circular cylinder was used as the duct. As has been previously mentioned, open-ended ducts have already been studied in great detail whereas ducts with two open ends have not been as extensively researched. To start we look at modifications to the measurement setup required for measuring the ducts. Then measurements and simulations of an open-ended duct are examined. Then a duct with two open ends is examined through measurement and simulation with a discussion of the differences compared to the open-ended duct.

3.2. MODIFICATIONS TO MEASUREMENT TEST-SITE

Measurements were taken using the test-site described in Chapter II. However, it was necessary to make some modifications to the test site in order to realize expected results. The RCS from an open-ended duct has previously been measured and simulated by Ram and Ling [27]. Initial measurements made on the test-site showed fewer late-time features that are caused by the modal behavior of the duct. The detailed physic of these late-time features will be discussed in more detail in section 3.3. The explanation for the discrepancy was that the return from the late-time phenomena fell below the noise floor. The solution was to increase the power of the signal in order to enhance the strength of the late-time scattering. Since the VNA has limited output power the only choice was to move the target closer to the measuring antennas, which would violate the plane-wave, far-field, and monostatic conditions discussed in Chapter II. For the RCS measurements

16

in this thesis the goal was to observe the backscattering phenomenology of the target as opposed to taking a measure of the absolute magnitude of the RCS of the target. Therefore it was acceptable to violate the far-field condition in favor of seeing the modal behavior of the duct.

As mentioned, moving the target closer violates the condition for the far-field, plane-wave, and monostatic measurement. Violating the far-field and plane-wave condition had a limited effect on the measured results, but the monostatic condition had a greater impact. In Figure 9 it was expected that there would a mode present above 14 GHz as in the previously reported results [27]. The modes that are excited, and the strength of each mode within the cavity is dependent on the incident angle of the excitation, therefore it was concluded that the higher order mode was not present because the antennas were no longer co-located. The solution was to measure the duct using one antenna instead of two antennas; therefore it would be guaranteed that the monostatic backscatter from the duct was being measured. Figure 10 shows the results of measuring an open-ended duct being with a single antenna. It is clear that by using one antenna the higher frequency mode is excited and observed. As discussed in Chapter II, the disadvantage of using one antenna is that the reflections from the antenna itself cannot be fully suppressed. However, since the target is sufficiently far away from the antenna the antenna reflections do not interfere with the measurement of the duct.
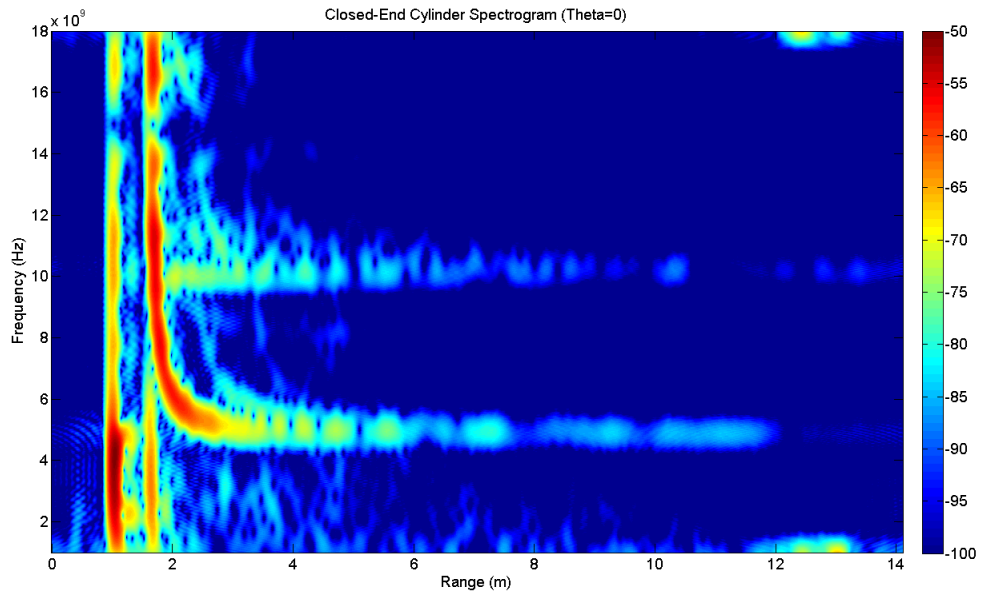
Figure 9 Measured spectrogram of open-ended duct with high order mode missing
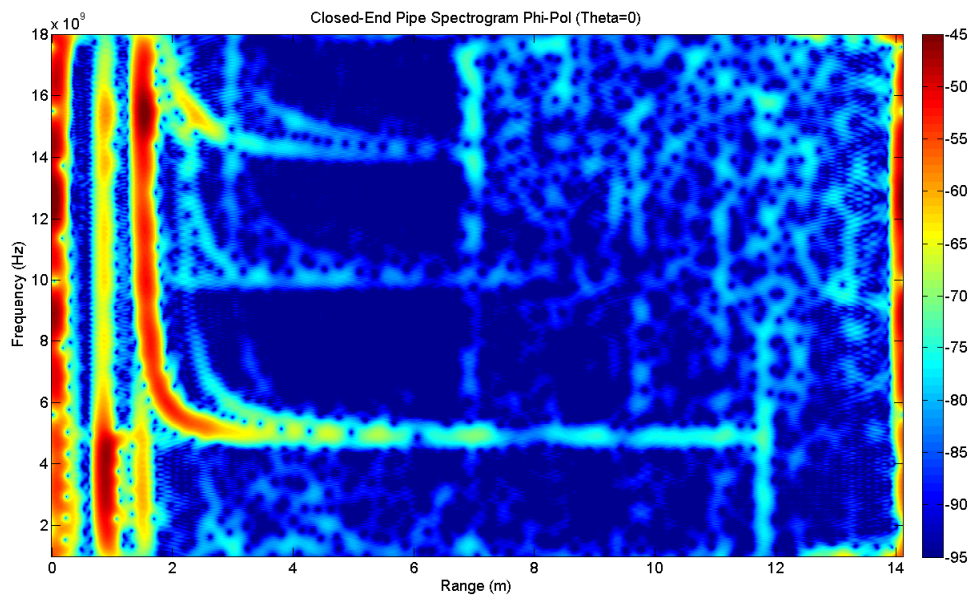
Figure 10 Measured spectrogram of open-ended duct with high order mode present and
excitation at boresight or theta equal to 0˚

3.3. OPEN-ENDED DUCT MEASUREMENT AND SIMULATION

Figure 10 shows the scattering from an open-ended duct where the measuring antenna is setup at boresight or theta equal to 0˚. Figure 14 shows the scattering from the open-ended duct when the antenna is moved in theta to approximately 45˚. Both measurement setups are illustrated in Figure 11. It is apparent that the duct will behave as a circular waveguide since a circular cylinder was used as the duct. Given that the duct acts as a waveguide it is possible to draw from the theory of waveguides to explain the scattering mechanisms of the duct.
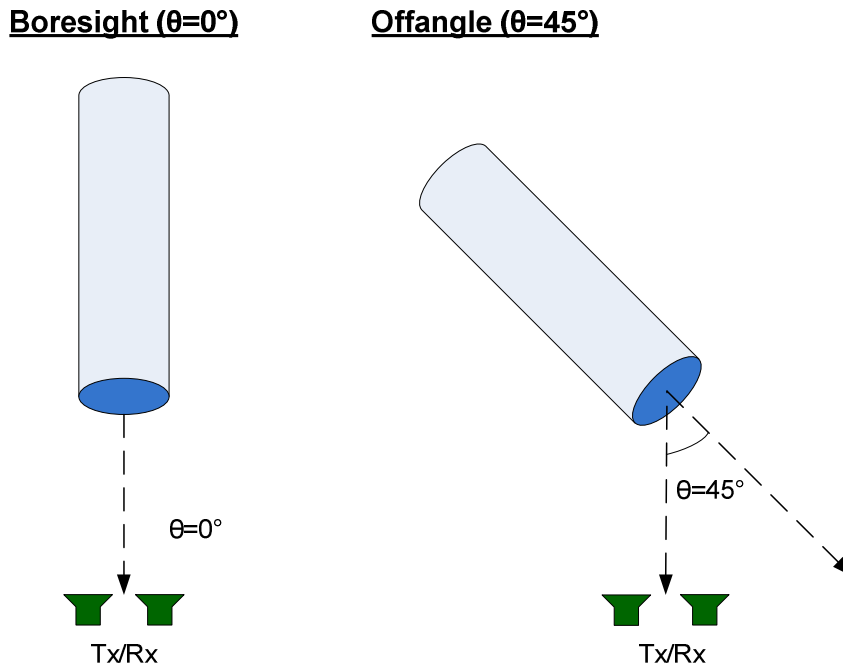
Figure 11 Measurement setup for ducts

It is known that for a given frequency the modes propagating within a waveguide can be determined by the respective cutoff frequencies for each mode. The cutoff frequencies for a circular waveguide can be calculated using equations (3.1) and (3.2) where: a, is the cross-sectional radius of the waveguide and χ_{mn} and χ'_{mn} represent the nth

zero of the Bessel function, J_m, and its derivative, J'_m, respectively. If none of the modes are above cutoff then no fields will propagate within the waveguide.

$$(3.1) \qquad (f_c)_{mn} = \frac{\chi'_{mn}}{2\pi a\sqrt{\mu\varepsilon}}$$

$$(3.2) \qquad (f_c)_{mn} = \frac{\chi_{mn}}{2\pi a\sqrt{\mu\varepsilon}}$$

When calculating the range to a target there is an intrinsic assumption that scattering from the target propagates at the speed of light. If any of the scattering propagates slower than the speed of light it will appear as though the target is farther away. In radar applications, backscatter from a target is a result of a pulsed plane-wave that impinges upon the target and scatters back toward the observer. Because the source is pulsed it is convenient to consider propagation speed in terms of the group velocity. The group velocity for a particular mode, equation (3.3), is a function of frequency. At frequencies close to cutoff the wave travels well below the speed of light approaching zero at cutoff, and approaches the speed of light when the operating frequency is significantly above cutoff. The conclusion is that when a mode is seen to be propagating within the duct, the range to any reflections will be a function of frequency. Near cutoff the target will appear as though it is much farther away and as the frequency increases the range will converge to the actual distance to target as seen in Figure 10.

$$(3.3) \qquad \left(v_g\right)_{mn} = c\sqrt{1 - \left(\frac{(f_c)_{mn}}{f}\right)^2}$$

The duct used for measurement has a radius of 1.9cm and length of 60cm shown in Figure 12. Using equations (3.1) and (3.2) the modes above cutoff can be determined in the frequency range extending from 1GHz to 18GHz, which corresponds to the bandwidth of the horn antenna used for measurement. Table 1 shows the propagating modes and their corresponding cutoff frequencies for a circular waveguide with radius

20

1.9cm. However, it should be noted that when a particular mode can be supported at a given frequency there is no guarantee that the mode will be excited. From Table 1 it can be seen that the lowest cutoff is 4.61 GHz corresponding to the TE_{11} mode. Below 4.61 GHz it is expected that no energy will couple into the duct.

Figure 12 Circular cylinder used for measurement of the open-ended duct and the duct with two open ends

TE$_z$	f$_c$ (GHz)	TM$_z$	f$_c$ (GHz)
TE11	4.61	TM01	6.02
TE21	7.65	TM11	9.60
TE01	9.60	TM21	12.86
TE31	10.52	TM02	13.83
TE12	13.35	TM31	15.98
TE22	16.80	TM12	17.57
TE02	17.57		

Table 1 Cutoff frequencies between 1 and 18 GHz for both TEz and TMz modes.

Since open-ended ducts have been extensively studied the scattering features from the duct are well understood. There are three main features to look for in the range profile of a duct that are depicted in Figure 13 [25]. In Figure 13 the three scattering features are labeled and correspond to 1: rim diffraction from the opening of the duct, 2: diffraction from the backend of the duct, and 3: modes that propagate through the duct and re-radiate from the opening.
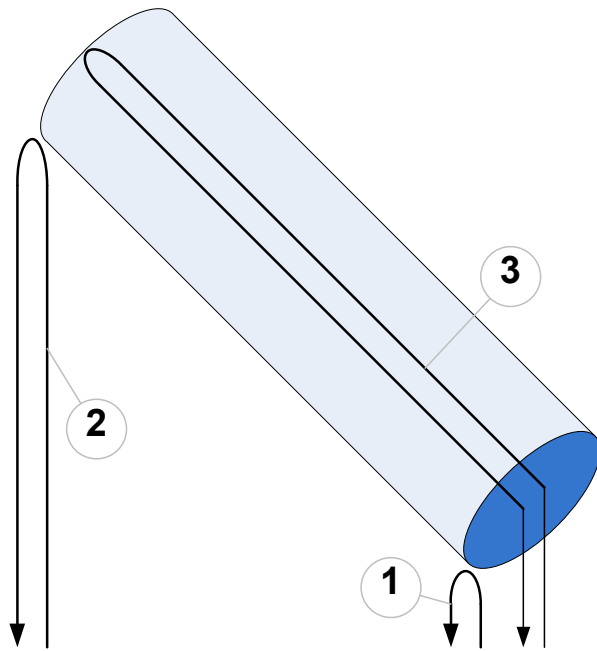
Figure 13 Scattering features from a duct

In the boresight measurement of the open-ended duct, Figure 10, the first feature is the reflection from the horn antenna used for measurement. The second feature is from the rim diffraction at the opening of the duct. It is interesting to note that the scattering from the opening is much stronger below cutoff, 4.61 GHz. The third feature is from the backend of the duct. Below cutoff the scattering is only from a traveling-wave propagating along the outside of the duct and reflecting off the backend. Once the frequency is above cutoff the scattering is a combination of the traveling-wave and reflections from the backend termination that propagated through the duct. At 4.61 GHz the characteristic tail from a mode can be observed which is asymptotic with the cutoff frequency of the particular mode. From Figure 12 it is clear that there are three tails present. The lowest mode corresponds to TE_{11} at 4.61 GHz, then there is a response corresponding to TE_{01} and TM_{11} at 9.60 GHz, and the highest mode observed is TE_{12} at 13.35 GHz. Clearly from Table 1 the duct supports far more modes, but as previously

23

mentioned, the presence of a particular mode is a function of the excitation. Therefore given a boresight excitation, only four modes are excited. The fourth set of scattering curves that converge to the same cutoffs as the previously mentioned modes correspond to double reflections within the duct. The scattering beyond 6 meters is not explained and should be ignored. This scattering is far beyond the measurement range and either corresponds to background clutter or interactions with the test equipment.

Figure 14 shows the scattering from the duct when the measuring antenna is moved 45˚ in theta. The most noticeable difference with the boresight measurement, Figure 10, is the presence of more modes. By moving the excitation in angle more modes have been excited. TE_{11}, TE_{01}, TM_{11}, and TE_{12} are still present. In addition the modes TE_{21} at 7.65 GHz and TE_{31} and 10.52 GHz are observed.
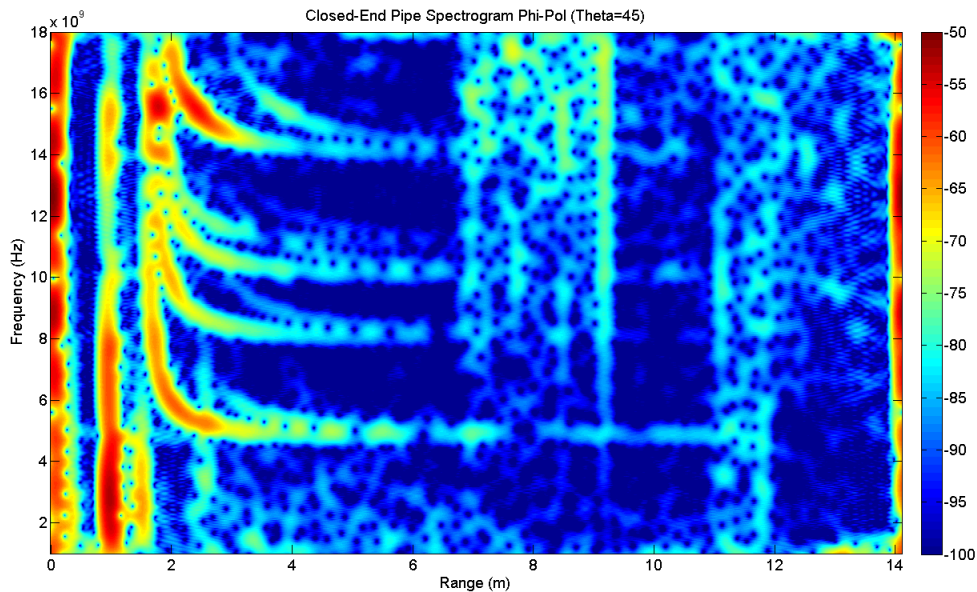

Figure 14 Open-ended duct with excitation at 45˚ with respect to boresight

The purpose of simulation in this thesis was to confirm that the measurements represent the phenomena that we anticipate and as a guideline for expectations in future measurements. Initial attempts were made to perform a rigorous solution of the open-ended duct using FEKO, which solves using the method of moments (MoM). However the memory requirements proved to be too large for a personal computer when a solution over 10 GHz was sought. Therefore the MoM solution was abandoned in favor of an approximation. The approximation used is based on equation (3.4), which was derived by Huang [18]. The derivation by Huang is for an open-ended circular cylinder, where the circular cylinder is treated as a waveguide. The basic premise of equation (3.4) is that an incident field, E_α^i, is applied from a particular direction and then the backscatter, E_α^s, is computed in the same direction. In the formulation each mode within the duct is expanded individually in terms of the incident field and propagated twice the length of the duct. The coefficient $S_{\alpha,nm}^2$ is the strength of each mode excited by the incident field, and its equation can be found in the references [18]. The coefficient $S_{\alpha\alpha}$ represents scattering due to the outside of the duct. For the simulations in this thesis the only scattering from the outside of the duct that is taken into account is the rim diffraction from the opening. The specific solution used for the rim diffraction is the asymptotic approximate to the Weiner-Hopf solution presented by Chuang, Liang, and Lee [15]. The reflection coefficient, Γ, is the reflection at the backend of the duct. In the case of the open-ended duct, the backend termination behaves as a short and has a reflection coefficient of -1.

$$(3.4) \qquad E_\alpha^s = \left[S_{\alpha\alpha} - \frac{j\pi}{kZ_o} \sum_n \sum_m S_{\alpha,nm}^2 \Gamma e^{-j2\beta_{nm}L} \right] E_\alpha^i \frac{e^{-jkR}}{R}$$

$$\alpha = \begin{cases} \theta \\ \varphi \end{cases}$$

25

Figure 15 and Figure 16 show the simulated spectrograms for the open-ended duct at 0° and 45° respectively. There are some key differences between the simulation and measured results shown previously. The initial return from the opening of the duct is different in that it does not decrease in magnitude once the frequency is above the cutoff for TE_{11}. An explanation for the difference is that the rim diffraction is computed using an approximation that assumes a high frequency, and therefore the approximation is invalid at lower frequencies. The second noticeable difference is that for the scattering from the backend of the duct there is no return below cutoff. As previously mentioned this scattering is a result of a traveling-wave propagating down the outside of the duct and reflecting off the back rim. Since the term $S_{\alpha\alpha}$ used in our simulation only accounts for the rim diffraction from the open end of the duct it is natural that we will not see any scattering resulting from the backend rim diffraction. The third difference between simulation and measurement is that in the boresight measurement the modes at 9.60 GHz corresponding to the TE_{01} and TM_{11} modes can be seen to propagate through the duct. In simulation these two modes are not present. As previously mentioned, the modes excited are a function of the excitation. Since the TE_{01} and TM_{11} modes are present in the offangle measurement the discrepancy in the boresight measurement is a result of inaccurately aligning the duct with the antenna for the boresight measurement. The last difference between measurement and simulation is the features in measurement that are attributed to double reflections within the duct. In simulation each mode is only propagated down the duct and back once, completing one round-trip through the duct. Any power that then completes a second round-trip will not be accounted for in simulation. Therefore the double reflections observed in measurement are not present in simulation. Despite the differences between measurement and simulation there is still

26

good agreement in the scattering mechanisms of the duct. In the offangle case the simulation predicts the excitation of the same modes that are seen in measurement.
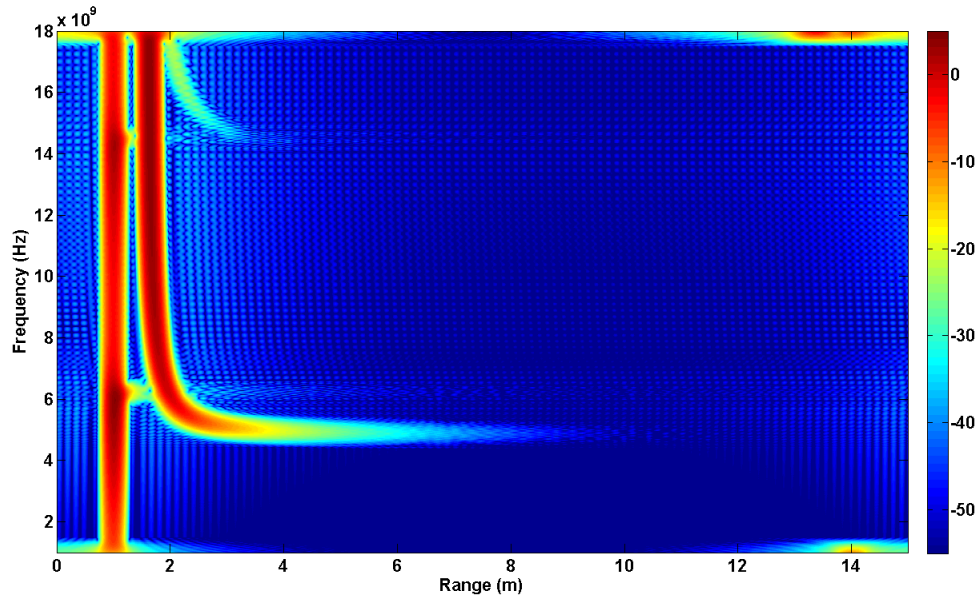

Figure 15 Open-ended duct simulation at boresight
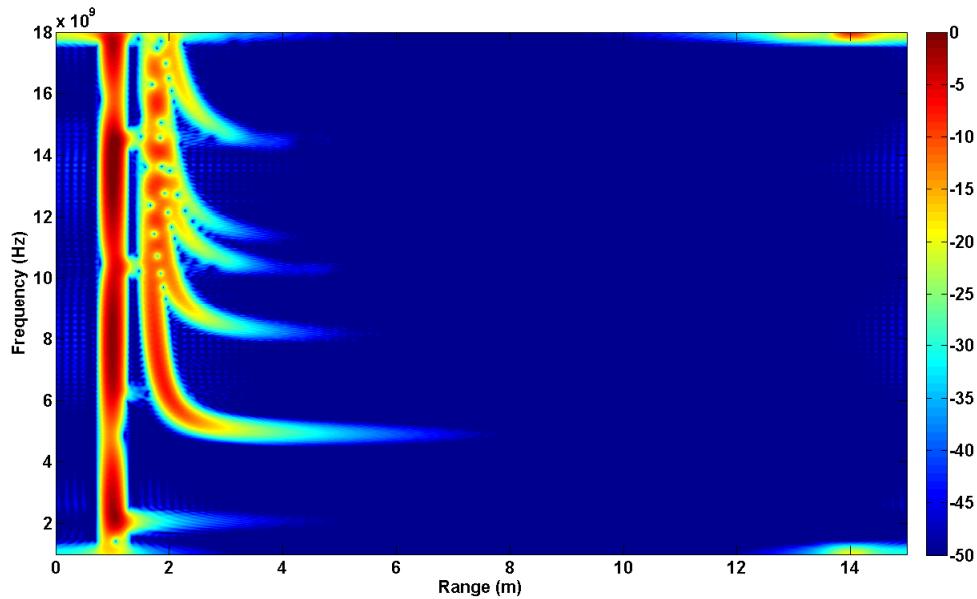
Figure 16 Open-ended duct simulation displaced 45 degrees in theta with respect to boresight

3.4. DUCT WITH TWO OPEN ENDS MEASUREMENT AND SIMULATION

In the duct with two open ends, the only physical difference is that the termination on the backend of the duct is opened, whereas before it was closed with a metal termination. It is expected that much of the same physics will apply to the duct with two open ends as applied to the open-ended duct. The duct will still behave like a circular waveguide the only difference being that when the modes propagating inside the duct reach the backend there will not be 100% reflection as before. The amount of energy reflected back remains to be seen.

Figure 17 shows the measured spectrogram for a duct with two open ends at boresight or 0° in theta. It should be noted that Figure 14, which depicts the open-ended duct measurement, is plotted on the same dynamic range and measured from the same

28

distance. Comparing open-ended to two open ends, the first feature from the opening of the duct is unaffected. The tails that are characteristic of each mode being excited can also been seen. The same modes are seen in both cases with the key difference being that as the frequency increases the scattering from each mode above cutoff is decreasing in strength. This provides insight into the nature of the open termination at the backed of the duct. When the mode propagates within the duct near cutoff it will tend to reflect from the open end termination at the back and as the frequency increases this reflection decreases, indicating that the modal impedance becomes better matched with free-space at higher frequencies.

Figure 18 shows the measurement for a duct with two open ends when the measuring antenna offset 45˚ in theta. The open-ended duct for comparison is shown in Figure 14, again both are plotted on the same dynamic range and measured from the same distance for a fair comparison. Much like the boresight measurement, there is very little difference in the scattering from the opening of the duct. The same modes are also excited and the dampening of the reflection from the backend for each mode as frequency is increased above cutoff can also be observed.
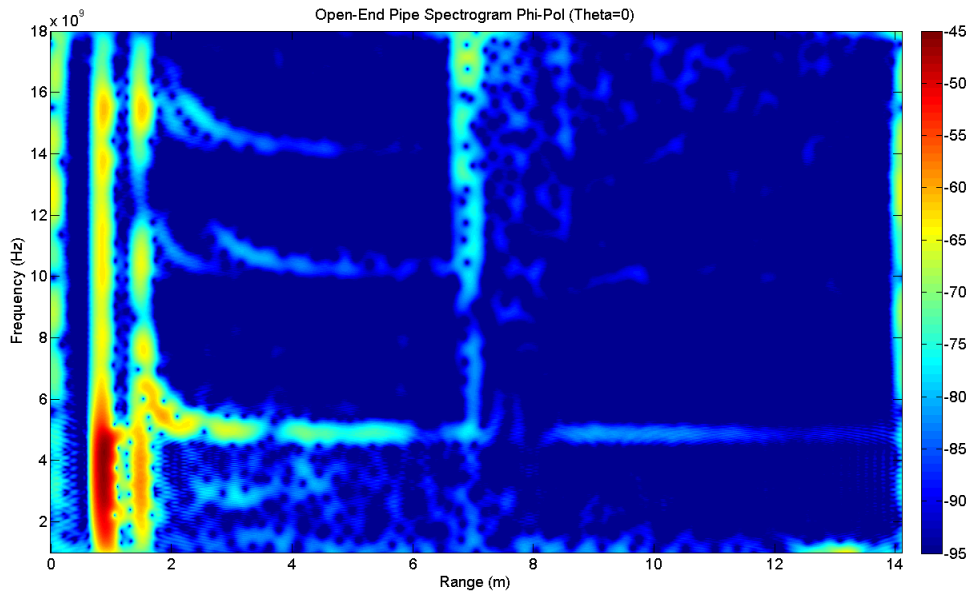
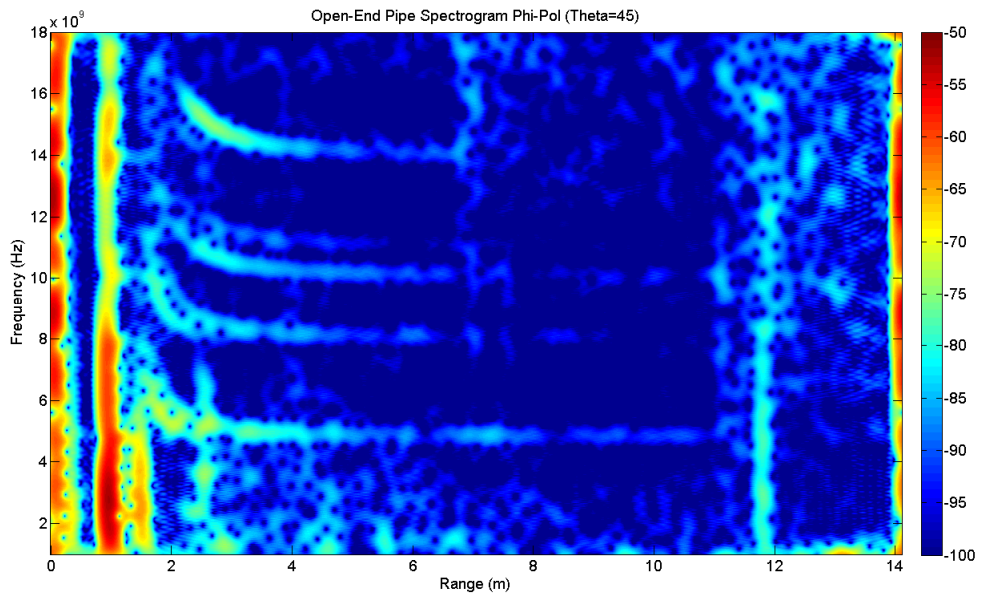Figure 17 Measured spectrogram of duct with two open ends at boresight

Figure 18 Measured spectrogram of duct with two open ends displaced 45 degrees with respect to boresight

As previously mentioned, the backend reflections can be observed to be a result of an impedance mismatch between free-space and the impedance of the wave traveling inside the duct. In the case of a shorted backend termination it is known the reflection coefficient is -1. In order to simulate the duct with two open ends the reflection coefficient needs to be computed using the appropriate impedances. The impedance of a particular mode can be computed using equation (3.5) for TE modes or equation (3.6) for TM modes. Since the simulation uses equation (3.4), which expands each mode individually, the reflection coefficient, Γ, can be computed for each mode using equation (3.7), where Zmn is the respective mode impedance and η is the free-space impedance as seen by the mode. For the purpose of this thesis η was set to η_o or 377Ω as a very rough approximation. Using η_o is inaccurate because it is the impedance of a plane-wave in free-space, however the field distribution at the opening of the duct will not be a plane-wave and therefore have an alternate impedance for the opening. For a more accurate solution a more realistic η would need to be used, or Γ would need to be solved for using a numerical method.

$$(3.5) \qquad Z_{mn}^{TE} = \frac{\omega\mu}{\sqrt{\beta^2 - \left(\frac{\chi'_{mn}}{a}\right)^2}}$$

$$(3.6) \qquad Z_{mn}^{TM} = \frac{\sqrt{\beta^2 - \left(\frac{\chi_{mn}}{a}\right)^2}}{\omega\varepsilon}$$

$$(3.7) \qquad \Gamma = \frac{\eta - Z_{mn}}{\eta + Z_{mn}}$$

Using the modified simulation the duct with two open ends was simulated for the boresight and offangle configurations. Figure 19 shows the boresight results, which as expected shows the TE$_{11}$ and TE$_{12}$ modes propagating through the cavity. Just as in the measurement we can also see that as the frequency increases above cutoff the reflection

31

from the mode grows weaker. Figure 20 shows the simulation when the incident source in move 45˚ in theta. This result also agrees well with measured results as we see the additional modes and the decreasing strength with frequency.
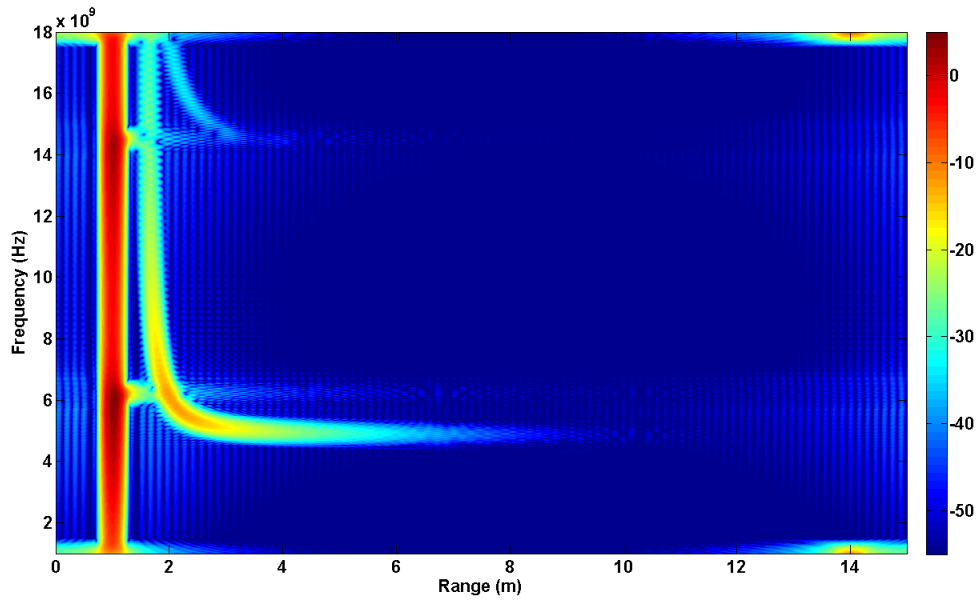

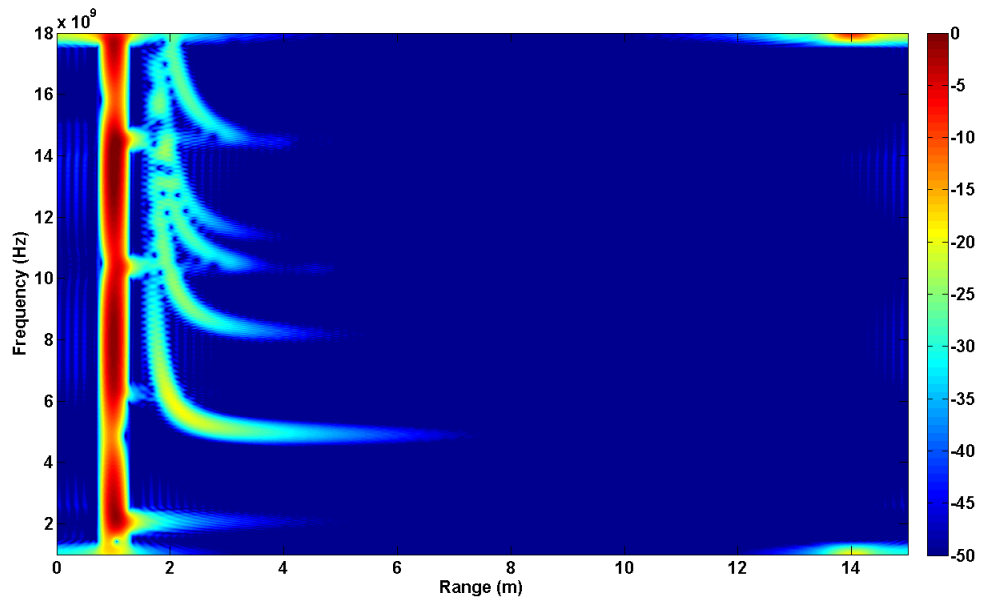Figure 19 Simulation of duct with two open ends at boresight

Figure 20 Simulation of duct with two open ends displaced 45 degrees in theta with respect to boresight

Chapter IV: Using Ducts for Through-the-Wall Propagation

4.1. INTRODUCTION

The premise of this chapter is to investigate the possibility of using a duct with two open ends as a means of looking through a wall using radar. There has been recent and continuing interest in the capabilities of through-the-wall radar systems [1-3]. One motivation behind through-the-wall radar is to gain a tactical advantage in urban combat situations. There is also the potential for applications in disaster search and rescue and law enforcement. Previous work has focused on characterizing the insertion loss of the wall [8-12]. The work done by Gibson and Jenn showed that a typical wall made out of concrete tends to act as a low-pass medium [8]. This implies that as the frequency increases the wall becomes more and more opaque to the radar. Consequently, most of the through-the-wall radar development has focused on frequencies below 5GHz. At lower frequencies and longer wavelengths, however, the ability to resolve finer details is sacrificed. The idea in this chapter is to accept that the wall will not allow good transmission and investigate whether it is possible to use a hole in the wall as a "radar pinhole" that will provide information about targets on the other side.

In Chapter III it was shown that a duct with two open ends reflects less power from the backend as the frequency increases well above cutoff. Since the power is not being reflected back to the receiver it must be radiating out the end. In this chapter we will look at whether or not that radiated power will scatter off a target, couple back into the duct, and then be received on the transmitting side of the duct. As with the rest of the thesis, this work will focus on measurement and use simulation to confirm the findings. The first section will discuss the wall used and its transmission loss. Measurements will then be made through the duct in an attempt to see a target on the other side of the wall. Modifications are then made to the simulation to replicate the measurement setup.

Finally, measured and simulated insertion loss through the duct is presented with a comparison made to through wall insertion losses reported in the literature.

4.2. MEASUREMENT SETUP

The goal of this experiment was to demonstrate and analyze the transmission capabilities of a duct with two open ends in the wall. Therefore the main concern was characterizing the transmission properties of the duct rather than the duct and wall. When building the wall the goal was not to reproduce a realistic wall, but instead we wanted a barrier that did not allow power to pass. Therefore a barrier was made using absorbers, shown in Figure 21. Figure 21 shows the wall with the duct already in place, for characterizing the transmission loss of the wall alone, the duct was removed. It was found that it was unnecessary to plug up the hole where the duct had been in order to prevent transmission.
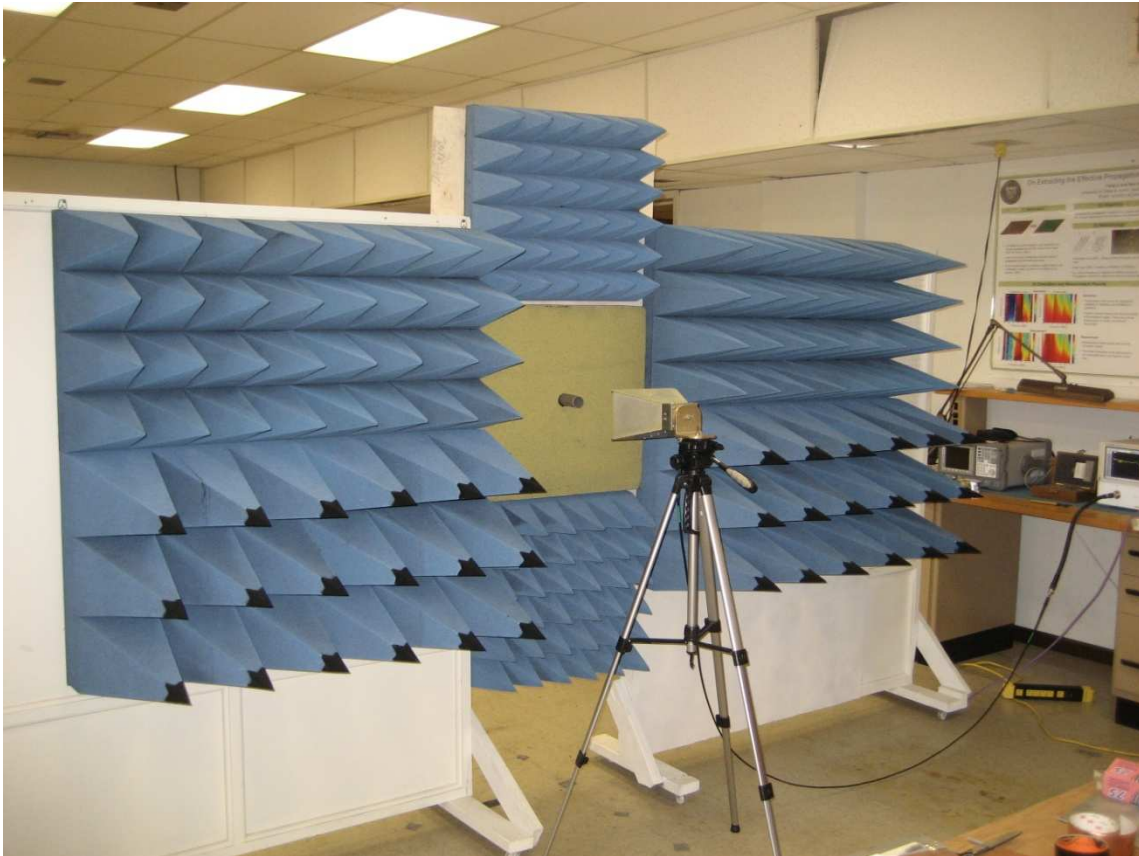
Figure 21 Absorbing wall

Having setup the absorbing wall it was then necessary to insure that the wall was sufficient to demonstrate the transmission capabilities of a duct with two open ends. By placing an antenna on both sides of the wall and measuring S_{21}, the transmission loss was determined. Figure 22 shows the measured transmission loss for the wall compared to free-space and compared to the case when the duct is inserted into the wall as shown in Figure 21. In Figure 22 the blue curve shows the transmission loss measured in free-space. Above 16 GHz it can be seen that transmission drops significantly which is due to errors in the measurements. SMA connectors were used for connecting the VNA to the measuring antennas. SMA connectors are only rated up to 18 GHz and have proven to be difficult to calibrate near 18 GHz, which causes errors in the measurement at higher

frequencies. The green curve, which shows the transmission loss of the absorbing wall, is clearly much lower than free-space. The red curve then shows the transmission loss when the duct is inserted in the wall. We recall that the first cutoff for our duct was 4.61 GHz. The transmission loss with the duct tracks the absorbing wall loss until 4.61 GHz is reached and then the transmission significantly increases, indicating that the duct is now propagating energy to the other side. The second mode that is cutoff at 14 GHz can be seen by the increased oscillation in the red curve after 14 GHz. One feature to note is that at the low end of the frequency range, the transmission through the wall is on par with the transmission through the duct above cutoff. It is not clear exactly what causes the transmission to be higher through the wall at lower frequencies, but one possibility is that the absorbers are not as effective at lower frequencies.
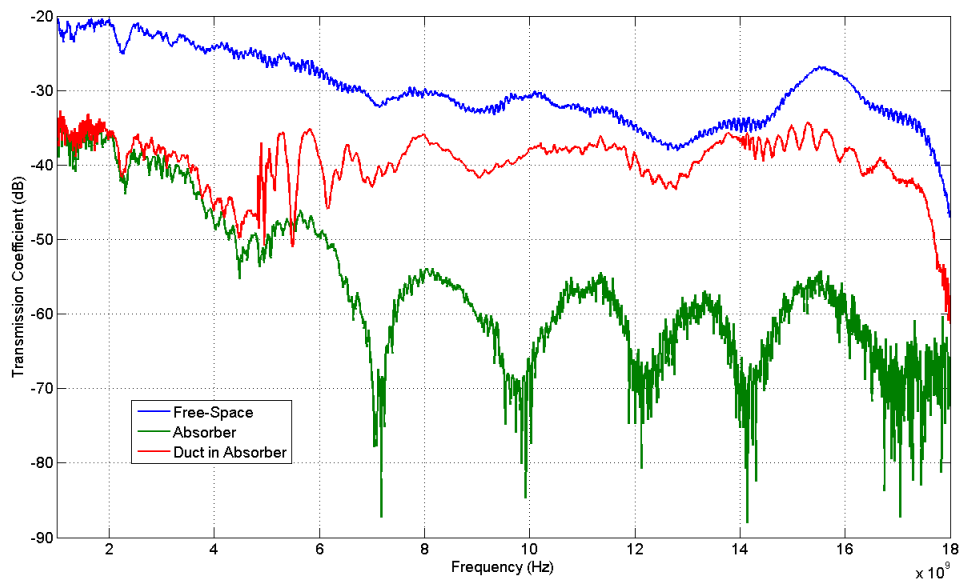

Figure 22 Transmission coefficient of experimental wall

4.3. MEASURED PROPAGATION THROUGH DUCT

Having verified that transmission is taking place primarily through the duct and not through or around the wall, the next step was to try and see a target on the other side of the wall. For the target, a corner reflector was chosen. Corner reflectors are convenient because they offer a large and angularly stable RCS. The primary goal of the experiment was to demonstrate that a target could be seen through the duct. A secondary goal was to also demonstrate that the target could be seen when the target and the receiver were not optically visible through the duct. Given these goals the configurations shown in Figure 23 were used. In each case a single antenna was used as in Chapter III to guarantee a monostatic measurement. The corner reflector is labeled as σ. Setup 1 is when both the measuring antenna and corner reflector are lined up at boresight, or theta equal to 0˚. For setup 2 the corner reflector is moved approximately 45˚ in theta, so that the target is not optically visible from the transmit and receive side of the duct. For setup 2 the measuring antenna is left at boresight. The inverse of setup 2 would be to leave the corner reflector at boresight and move the antenna 45˚ in theta, but by reciprocity we know the results would be the same. Setup 3 is configured so that both the corner reflector and the antenna are moved 45˚ in theta. The exact configuration shown in Figure 23 was used so that the corner and antenna were not facing each other.
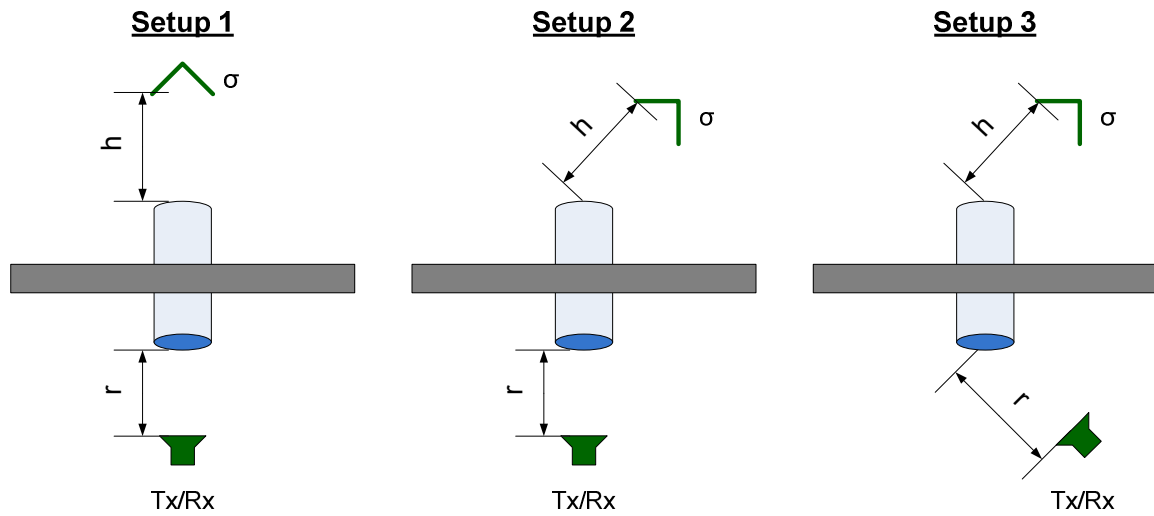
Figure 23 Configurations for through-the-wall measurements

As mentioned, the RCS measurements were taken using one antenna, shown in Figure 24. As before the measurements were made using background subtraction. In this case the background includes the wall and the cavity. Therefore the only difference between the target measurement and the background measurement is the presence of the corner reflector. The implication is that when looking at the range profile the scattering from the duct will not be present, only the effects of the duct on the scattering from the corner reflector will be seen.

Figure 24 Transmit and receive using one horn antenna for Setup 1
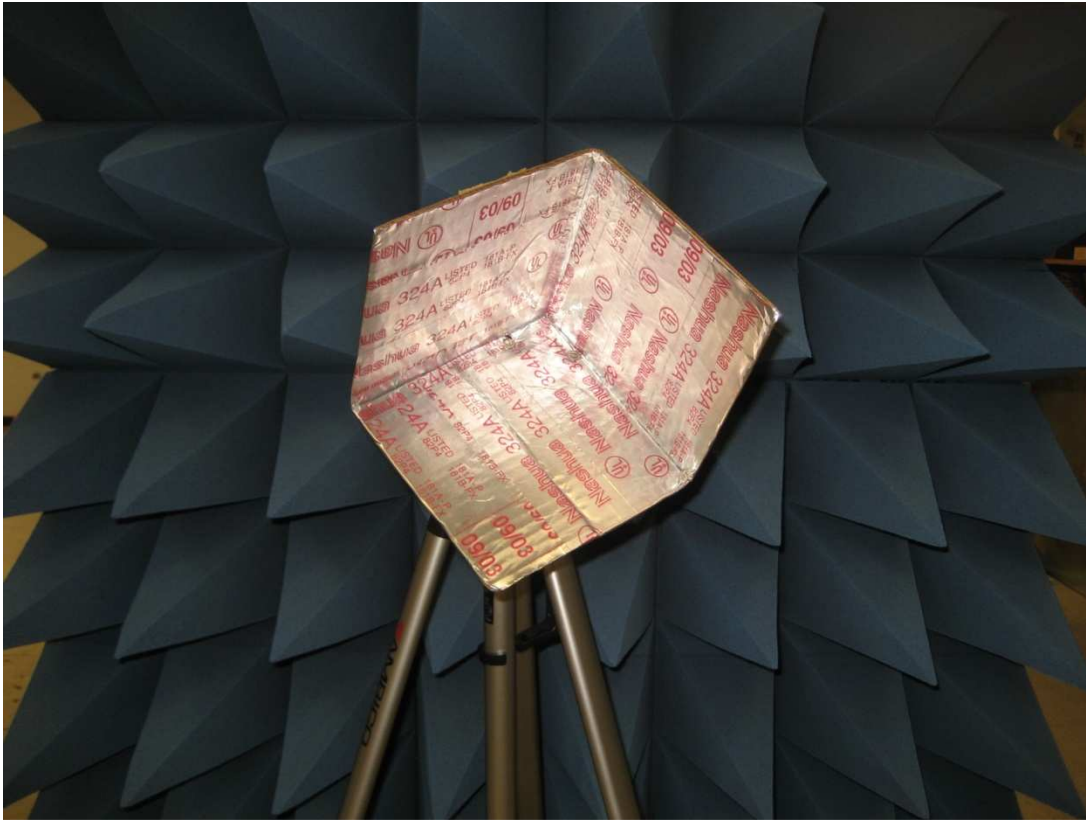
Figure 25 Corner reflector used as target on opposite side of wall

Figure 26 shows the spectrogram from the measurement made using setup 1 in Figure 23. The first reflections at around 0m down-range are again the result of reflections in the antenna that could not be fully su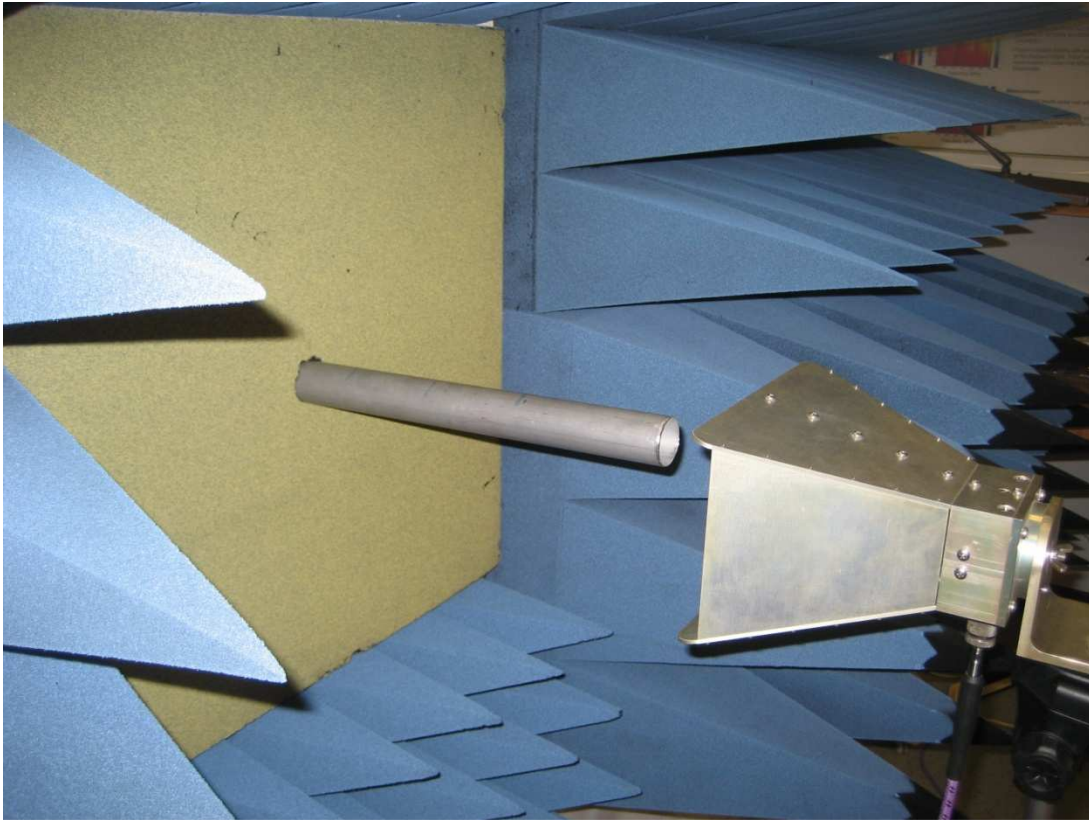ppressed using background subtraction. The second return is from the corner reflector. The antenna was placed about 20cm from the duct, which is 60cm long, and the corner reflector was placed a further 80cm from the duct. Based on these numbers it is evident that the second reflection is not from the duct itself. The return below cutoff is due to the low transmission loss for lower frequencies that were observed in Figure 22. It is confirmed that the scattering from the corner reflector is propagating through the duct by making two observations. Referring back to the transmission loss measurements in Figure 22, we see that for higher frequencies the absorbing wall did not allow power to pass, therefore any scattering seen

on the other side of the wall must be coupling through the duct. The second observation that indicates the scattering is propagating through the duct is that the return shows the characteristic tail of a dispersive medium, which in this case is the duct. It is also possible to say that two modes are carrying the energy through the duct, TE_{11} and TE_{12}. From previous results it might be expected that TE_{01} and TM_{11} would also carry energy. Since the return from those particular modes was weak in the open-ended duct, Figure 10, it is possible that those modes have fallen below the noise floor or the antenna is better aligned with the duct and the modes are not excited. Again, the scattering beyond 6 meters should be ignored as this is well beyond the target of interest.
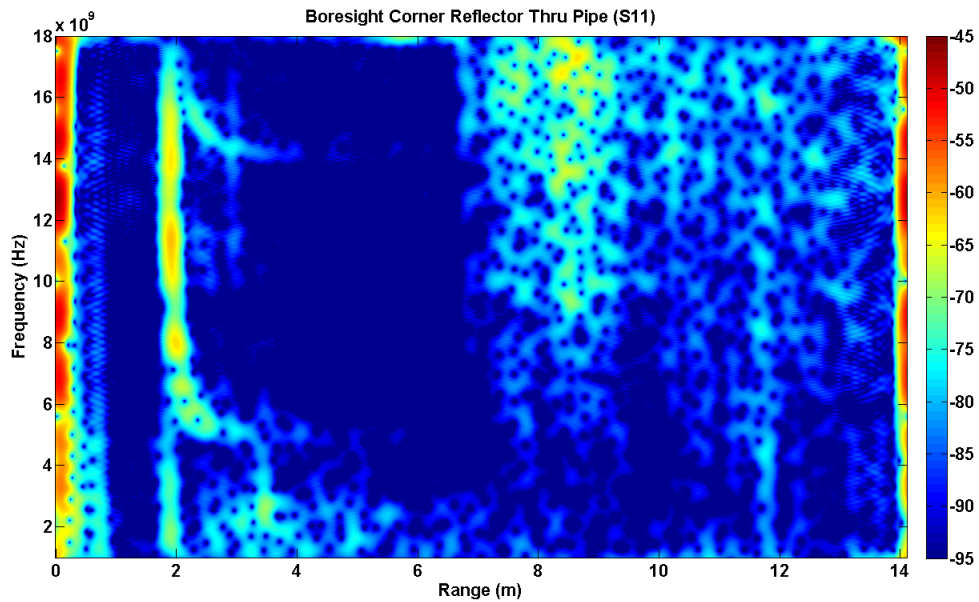

Figure 26 Spectrogram showing scattering of corner reflector using Setup 1

Figure 27 shows the measurement results from setup 2. The shape of the spectrogram is similar to Figure 26. However the magnitude of the scattering is weaker in Figure 27. If the backend of the duct is treated as an aperture it follows that it would have

a beam pattern associated with the far-field radiation. If the main-beam is at a maximum at boresight, or theta equal to $0°$, it follows that the scattering would be weaker for setup 2 since the corner reflector is no longer being illuminated by the main-beam. The actual beam pattern is a function of the field distribution on the aperture, which will depend on the modes excited within the duct. Just as in setup 1, the power in setup 2 is being propagated by TE_{11} and TE_{12}. One might expect to see more modes propagating within the duct since the corner reflector has been moved in theta, but that is not the case. From the results in Chapter III it is known that when the transmitting antenna is positioned at boresight TE_{11} and TE_{12} are excited. If the field is then observed on the opposite side of the duct only TE_{11} and TE_{12} would be observed for all observation angles. Then by reciprocity we know that if the transmitting antenna is at any angle and the observer is at boresight only TE_{11} and TE_{12} would be observed. The RCS measurement is a combination of both situations and is the reason only two modes are seen.
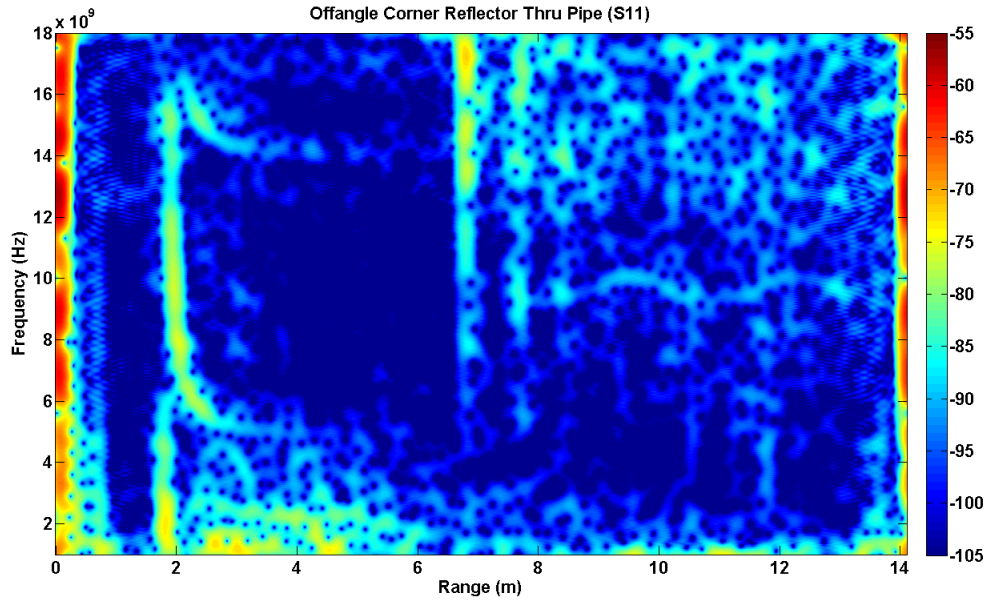
Figure 27 Spectrogram showing scattering of corner reflector using Setup 2

The final measurement was made using setup 3, where both the corner reflector and measuring antenna are moved approximately 45° in theta. Figure 28 shows the resulting spectrogram. The corner reflector can be seen, but an even greater drop in the magnitude is observed compared to the first two measurements. It can also be seen that more modes are now propagating through the cavity which correspond to the modes seen in the off-angle duct measurements made in chapter III.
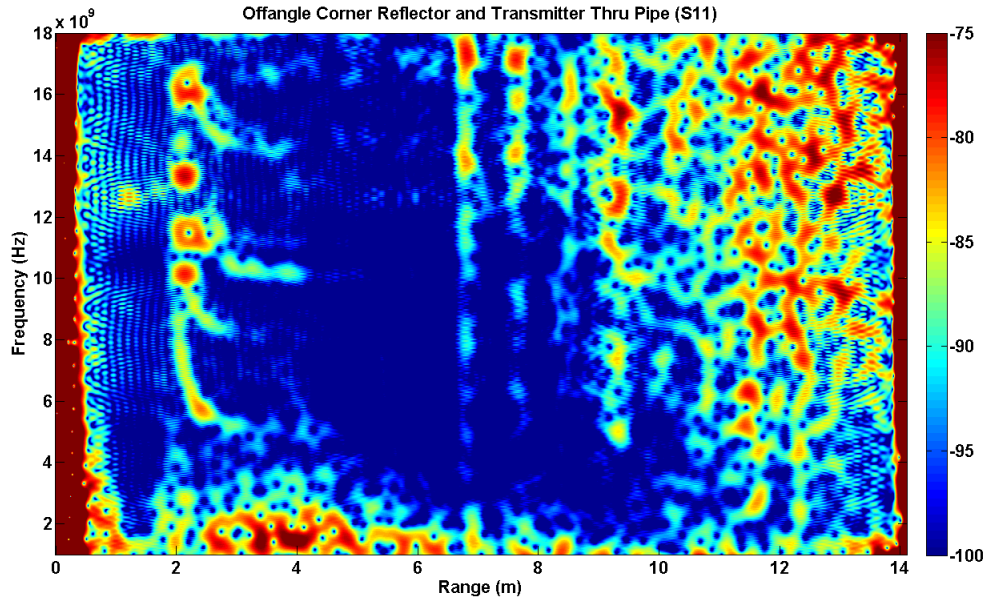
Figure 28 Spectrogram showing scattering of corner reflector using Setup 3

4.4. SIMULATED PROPAGATION THROUGH DUCT

The code used in the previous chapter was again modified for the measurements in this chapter. Previously the code took an excitation field from a particular direction, expanded the field in terms of the modes above cutoff, propagated the modes down the duct, reflected from the end termination, propagated back down the duct, and then computed the radiated field in the direction of the excitation field. The modification necessary was instead of reflecting from the end termination the new code radiates out the backend, reflects off the corner reflector, and then couples back into the duct. By modifying equation (3.4) to only propagate down the pipe and then radiate out the backend the result is equation (4.1). Using equation (4.1), the field incident on the corner reflector, E^I, can be computed where L is the length of the cavity and h is the distance from the cavity to the corner reflector, as shown in Figure 23.

$$(4.1) \quad E_\alpha^1 = \left[-\frac{j\pi}{kZ_o} \sum_n \sum_m S_{\alpha,nm}^2 e^{-j\beta_{nm}L} \right] E_\alpha^i \frac{e^{-jkh}}{h}$$

45

The next step is to compute the field incident on the duct as a result of scattering from the corner reflector. Equation (4.2) computes the field reflected from the cavity, E^2, in terms of the RCS of the target. The RCS of a corner reflector can be computed using equation (4.3) where b is the edge length of the corner reflector. The final scatter field, E^s, is then computed using equation (4.4), where r is the distance between the source and duct as shown in Figure 23.

$$(4.2) \quad E_\alpha^2 = \frac{\sqrt{\sigma}}{\sqrt{4\pi h}}|E_\alpha^1|e^{-jkh}$$

$$(4.3) \quad \sigma = \frac{12\pi b^4}{\lambda^2}$$

$$(4.4) \quad E_\alpha^s = \left[-\frac{j\pi}{kZ_o}\sum_n\sum_m S_{\alpha,nm}^2 e^{-j\beta_{nm}L}\right]E_\alpha^2\frac{e^{-jkr}}{r}$$

The qualification that comes with this formulation for computing the scattering through the duct is that in equations (4.1) and (4.4) the incident field and scattered field are assumed to be in the same direction. This means that the above modification to the simulation can be used to simulate setup 1 and 3 from Figure 23, but not setup 2.

The simulation was carried out using the dimensions from the measurement. The distance from the antenna to the duct, r, was set to 20cm, the length of the duct was 60cm, and the distance from the duct to the corner reflector, h, was set to 80cm. The edge length of the corner reflector, b, was set to 17cm. Rim diffraction from the duct was turned off so that there would be no scattering from the duct itself, only reflections from the corner reflector. When making measurements the phase reference is at the feed connection of the measuring antenna. The propagation through the antenna itself will add distance to the range profile of the target. Propagation through the antenna is assumed to be in free-space and lossless. For the horn antenna used in this thesis an additional 30cm is added. Figure 29 shows the simulated spectrogram that is equivalent to setup 1. Just as

46

in the measurement, Figure 26, the dispersion due to the duct can be seen and the propagating modes are clearly TE_{11} and TE_{12}. Figure 30 shows the simulated results for setup 3. The magnitude is about 20 dB lower which we anticipate from measurement and it is also clear that the scattering from the corner is being propagated through the duct by additional modes.
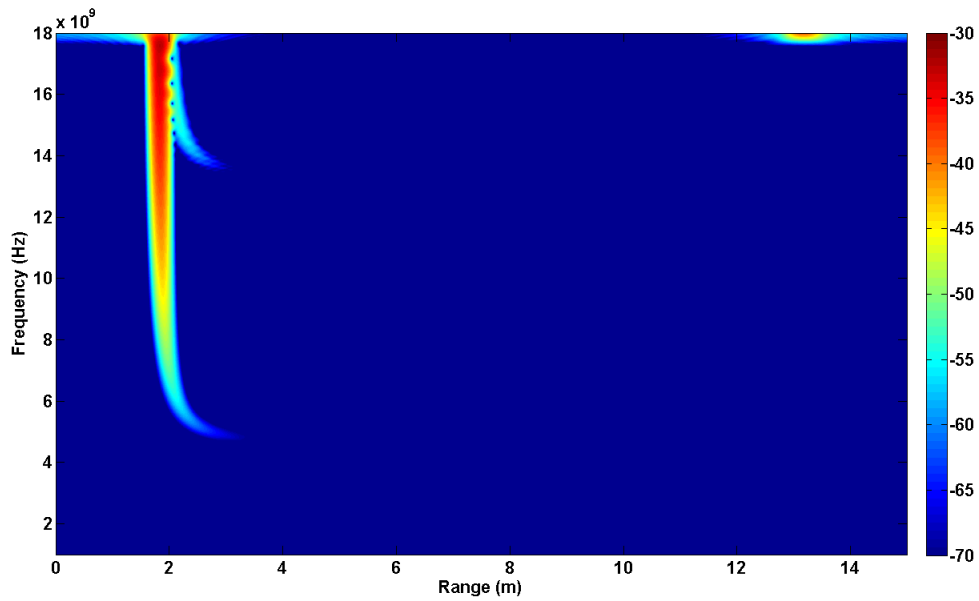
Figure 29 Simulated spectrogram of corner reflector through duct using Setup 1
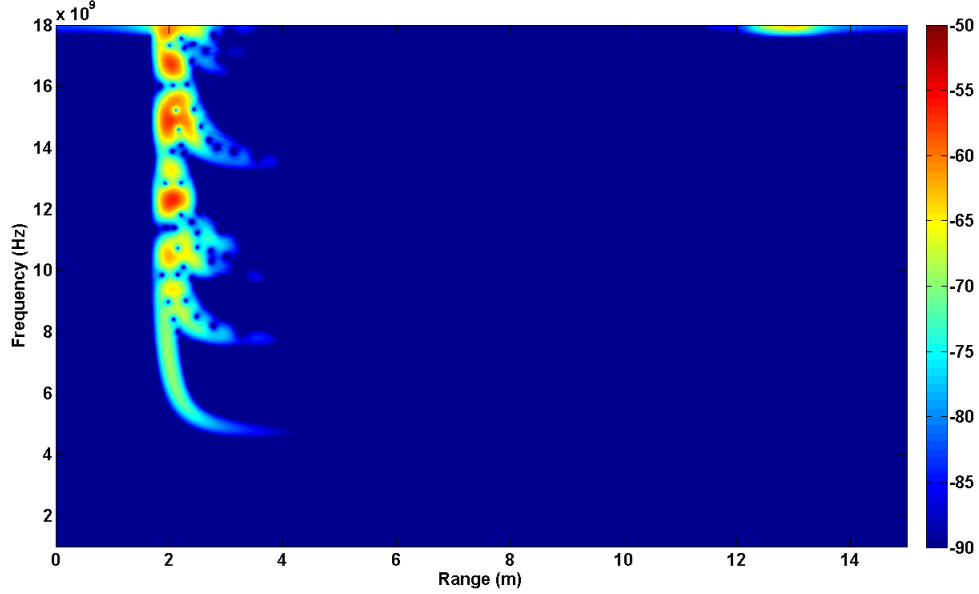
Figure 30 Simulated spectrogram of corner reflector through duct using Setup 3

4.5. TWO-WAY DUCT INSERTION LOSS

In order to characterize the quality of a duct as a transmission link through the wall the insertion loss is determined. The insertion loss is determined by computing the ratio of the power received when propagating through the duct and the power received when propagating in free-space, equation (4.5)

$$(4.5) \quad IL = \frac{\left|E_{duct}^{S}\right|^2}{\left|E_{free-space}^{S}\right|^2}$$

What follows are three different methods for determining the insertion loss due to the duct. The first formulation is purely analytical and makes some key assumptions that will lead to an optimistic estimate of the insertion loss. First the power received in free-space is determined using a form of the radar range equation, equation (4.6). In equation (4.6) r, L, and h correspond to the distance from source to duct, length of the duct, and

48

distance from the duct to target respectively. G_r and G_t are the gain of the transmit and receive antennas, σ is the RCS of the target, and P_t is the transmitted power.

$$(4.6) \quad P_{r,free-space} = \frac{\lambda^2 G_r G_t \sigma P_t}{(4\pi)^3 (r+L+h)^4}$$

In determining the power received when propagating through the duct some assumptions are made about how to handle the duct. The first assumption is that all the power captured by the duct is propagated to the other end at the same speed. Another assumption is that the duct accepts and radiates all the power within its capture area. In reality this is not the case as there are reflections each time the fields enter or leave the duct. The final expression for the power is given by equation (4.7), where A is the capture area or cross-sectional area of the duct.

$$(4.7) \quad P_{r,cavity} = \frac{\lambda^2 G_r G_t \sigma P_t}{(4\pi)^3} \cdot \frac{A^4}{\lambda^4 r^4 R^4}$$

Taking the ratio of the power received through the duct and the power received through free-space gives an expression for the insertion loss, equation (4.8).

$$(4.8) \quad IL = \frac{P_{r,cavity}}{P_{r,free-space}} = \left(\frac{A(r+L+h)}{\lambda r h}\right)^4$$

The second formulation for the insertion loss due to the duct uses the electromagnetic simulation from the previous section. The scattered field with the duct can already be computed without modification. The only additional information needed is the scattered field in free-space given the same dimensions and same incident field, equation (4.9). The final expression for the insertion loss is given by equation (4.5), where E^S_{cavity} is the scattered field determined through simulation.

$$(4.9) \quad E^S_{free-space} = \frac{\sqrt{\sigma} \cdot r}{\sqrt{4\pi} \cdot (r+L+h)^2} \left|E^i_\alpha\right| e^{-jk(2(L+h)-r)}$$

The third and final expression for the insertion loss uses measured results from section 4.3 and a measurement of the corner reflector in free-space, with the same distance between antenna and target. The resulting measurements are used to compute the insertion loss using equation (4.5). Figure 31 shows the insertion loss resulting from each formulation for setup 1. The green curve shows the insertion loss computed from the first formulation in equation (4.8), the red curve is the simulated insertion loss from the second formulation, and the blue is the measured results. In making comparisons between measured and simulated results it is not necessary to know the gain of the transmit and receive antennas due to the normalization with respect to free-space. As expected, the green curve gives an optimistic insertion loss, which serves as an upper bound for the results. The simulated (red) and measured (blue) results agree very well, especially near the first cutoff, 4.61 GHz. The oscillation in the measured results near the first cutoff is due to interference with an unknown scattering feature. The unknown feature could be scattering that passes through the wall due to the imperfect absorbers. The oscillation in the simulated results that occurs after 13 GHz is due to interference between the TE_{11} and TE_{12} modes. At this point the measured results begin to deviate from the simulation. However the measurements made at higher frequencies are approaching the limit of the SMA connectors and the horn antenna used. The limitations of the measuring equipment leads to the drooping seen in the measured results at higher frequency. Figure 32 shows the insertion loss for setup 3, where both the measuring antenna and corner reflector are at 45° in theta. The insertion loss is clearly much higher for setup 3, which should be expected based on results in previous sections. In the end it is possible to come to the conclusion that our simulation gives an accurate depiction of the insertion loss due to the duct. This assertion is based on the agreement between simulation and measured results shown in Figure 31 and Figure 32.
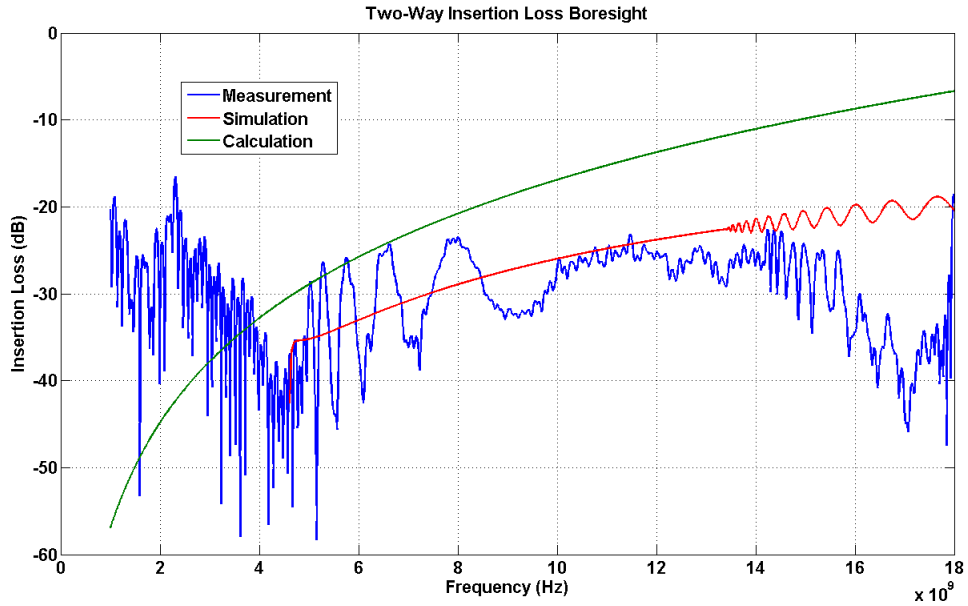
50

Figure 31 Two-way insertion loss through the duct, computed and measured, for Setup 1

Figure 32 Two-way insertion loss through the duct, computed and measured, for Setup 3

Finally, a comparison is made between the insertion loss due to the duct and the insertion loss of a wall that was previously published [8]. The wall presented in [8] was a 1ft thick concrete wall, and the insertion loss is based on both simulated and measured results. In the reference, the insertion loss presented is for the one-way path through a wall, whereas the results in this thesis are for the two-way path. Therefore the numbers extracted from [8] in decibels are doubled. There is one critical difference between the insertion loss due to a wall and the insertion loss due to a duct. For a wall the insertion loss is a factor of the wall material and the thickness of the wall, and it is independent of the distance from the wall for either the source or the target. For the duct however the insertion loss is a factor of the radius of the duct, the distance from source to the duct, and from the duct to the target. The influence of each parameter can be inferred from equation (4.8). Because the factors involved in the insertion loss for the two cases are independent of each other it is not possible to make an all encompassing statement about whether it is better to propagate through a duct in the wall or just the wall alone. What is possible is to show that given a specific situation or set of constraints it can be more beneficial to propagate through a duct. In Figure 33 this comparison is made, where the radar is set 20cm from the duct and the target is 10m away from the duct. The red curve shows the insertion loss as presented by Jenn and Gibson [8]. The green, black, and blue curves show the insertion loss through the duct as predicted by simulation for a 4.5cm-, 5.5cm-, and 6.5cm-radius duct. It is clear that a larger radius is more appealing in terms of insertion loss. It is also clear that for a given radius, the insertion loss improves with frequency. This is in contrast to a typical wall, for which the transmission becomes more difficult as frequency is increased.
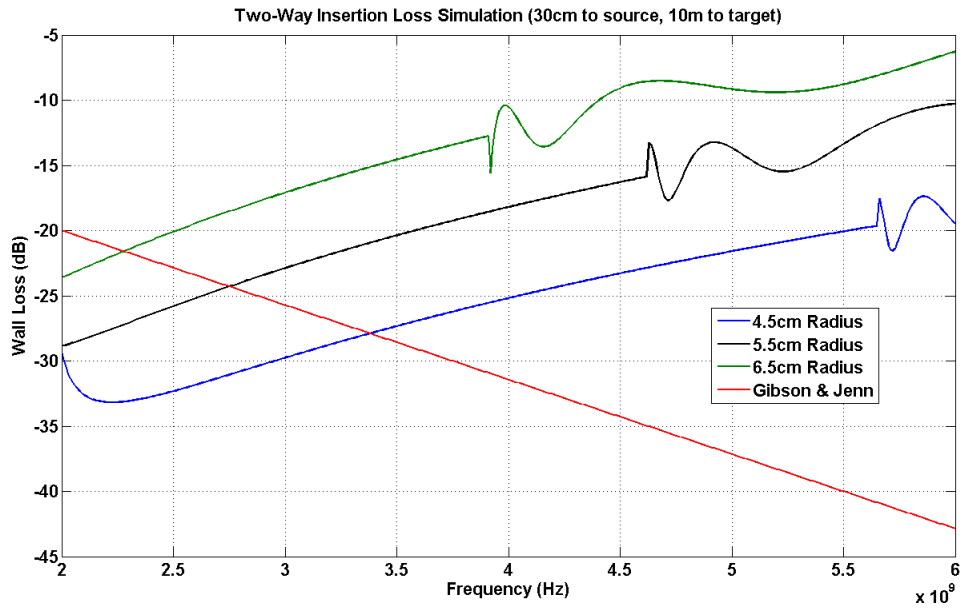
Figure 33 Two-way insertion loss of duct with two open ends compared to concrete wall

Chapter V: Conclusions

In this thesis a proper measurement test-site was devised in order to make measurements on ducts. A sphere was used to verify that the proper electromagnetic phenomena could be seen in measurements. The goal of the test-site was not to make accurate RCS measurements in dBsm, but rather to observe electromagnetic phenomena such as the creeping wave on the sphere. Having devised an appropriate method for making measurements an open-ended duct was measured and simulated. The results were then compared to previously published results. A duct with two open ends was then measured and simulated, and comparisons were made with the open-ended duct. It was noted that there was significant transmission through the duct at frequencies well above cutoff. The analysis of the duct with two open ends and the observation of high transmission motivated the idea of using a duct as a means of looking at targets on the other side of a wall, rather than by transmitting through the wall itself.

An experiment was then performed to show that a target could be observed through a duct with two open ends. Measurements were made that successfully observed a corner reflector through the duct. Simulations were performed to replicate the measured scenario and the two-way insertion loss between simulation and measurement was shown to be in good agreement. Using the simulation a comparison was made between previous work done on through-the-wall insertion loss and the insertion loss using a duct in the same frequency band. It was found that while through-wall propagation becomes increasingly more difficult at higher frequencies, the duct works increasingly better at higher frequencies. The conclusion made was that given the appropriate circumstances it would be better to propagate through a duct, than trying to pass through the wall itself.

There are further studies that could possibly stem from this work. The first is to modify the simulation so that the excitation source and target can be at different incident angles. With a bistatic simulation the beam pattern of the radiated field from the duct could be analyzed, which could potentially explain the significant loss when the source and target are both moved 45˚ in theta. An analysis of duct that are not made of metal, such as PVC pipe, would be interesting as that would be more common to find embedded in a wall. Looking at Doppler signatures through the duct could be of interest for detecting moving objects such as humans. Doppler discrimination may offer processing gains that could compensate for the cases of high insertion loss. A study of how well the modes will follow the duct around bends would be interesting as that may open the possibility of using air ducts as a means of getting a radar picture of the inside of a building. There are undoubtedly more experiments that could follow from this work and potentially other scenarios that exploit or necessitate the understanding of the RCS from a duct with two open ends.

Bibliography

[1] DARPA Strategic Technology Office, "STO: Visibuilding," Available: http://www.darpa.mil/sto/smallunitops/visibuilding.html. [Accessed: July 16, 2009].

[2] National Institute of Justice, "Through-the-Wall Surveillance: A New Technology for Saving Lives," *NIJ Journal No. 258, Oct. 2007*, Available: http://www.ojp.usdoj.gov/nij/journals/258/through-the-wall-surveillance.html. [Accessed. July 16, 2009].

[3] DARPA Strategic Technology Office, "Comprehensive Interior Reconnaissance," Broad Agency Announcement, DARPA-BAA-09-38, March 31, 2009.

[4] S. Nag, M. A. Barnes, T. Payment, and G. W. Holladay, "An Ultra-Wideband Through-Wall Radar for Detecting the Motion of People in Real Time," *SPIE Proceedings,* vol. 4744, pp. 48-57, 2002.

[5] A. R. Hunt, "A Wideband Imaging Radar for Through-the-Wall Surveillance," *SPIE Proceedings,* vol. 5403, pp. 590-596, 2004.

[6] A. R. Hunt and R. D. Hogg, "A Stepped-Frequency, CW Radar for Concealed Weapon Detection and Through the Wall Surveillance," *SPIE Proceedings,* vol. 4708, pp. 99-105, 2002.

[7] S. Ram, L. Yang, A. Lin, and H. Ling, "Doppler-Based Detection and Tracking of Humans in Indoor Environments," *Journal of the Franklin Institute,* vol. 345, pp. 679-699, Sept. 2008.

[8] T. B. Gibson and D. C. Jenn, "Prediction and Measurement of Wall Insertion Loss," *IEEE Trans. on Antennas and Propagat.,* vol. 47, no.1, pp. 55-57, Jan. 1999.

[9] M. Dehmollaian and K. Sarabandi, "Refocusing Through Building Walls Using Synthetic Aperture Radar," *IEEE Antennas Propagat. Soc. Int, Symp. Digest*, pp. 1465 – 1468, June 2007.

[10] V. Schejbal, P. Bezousek, D. Cermak, Z. Nemec, O. Fiser, and M. Hajek, "UWB Propagation Through Walls," *Radioengineering,* vol. 15, no.1, pp. 17-24, April 2006.

[11] A. Muqaibel and A. Safaai-Jazi, "Characterization of Wall Dispersive and Attenuative Effects on UWB Radar Signals," *Journal of the Franklin Institute,* vol. 345, pp.640-658, Sept. 2008.

[12] G. Greneker and E. O. Rausch, "Wall Characterization for Through-the-Wall Radar Applications," *SPIE Proceedings,* vol. 6947, pp. 1-11, 2008.

[13] H. R. Witt and E. L. Price, "Scattering From Hollow Conducting Cylinders," *IEE Proceedings,* vol. 115, pp. 94-99, Jan. 1968.

[14]   J. J. Bowman, "Scattering of Plane Electromagnetic Waves from a Semi-Infinite Hollow Circular Pipe," Conductron Corp., Ann Arbor, Mich., Memo D0620-125-M41-10 and Memo D0620-127-M41-13, 1963.

[15]   C. A. Chuang, C. S. Liang, and S. W. Lee, 'High Frequency Scattering from an Open-Ended Semi-Infinite Cylinder,' *IEEE Trans. on Antennas and Propagat.*, vol. ap-23 no. 6, pp. 770-775, Nov. 1975.

[16]   T. W. Johnson and D. L. Moffatt, "Electromagnetic Scattering by Open Circular Waveguides," *Radio Science,* vol. 17, no. 6, pp. 1547-1556, Nov.-Dec. 1982.

[17]   L. N. Medgyesi-Mitschang and C. Eftimiu, 'Scattering from Wires and Open Circular Cylinders of Finite Length Using Entire Domain Galerkin Expansions,' *IEEE Trans. on Antennas and Propagat.,* vol. ap-30, no. 4, pp. 628-636, July 1982.

[18]   C.-C. Huang, "Simple Formula For The RCS Of A Finite Hollow Circular Cylinder," *Electronic Letters,* vol. 19, no. 20, pp. 854-856, Sept. 1983.

[19]   C. W. Chuang, P. H. Pathak, and R. J. Burkholder, "A Hybrid Asymptotic Modal-Moment Method Analysis of The EM Scattering By 2-D Open-Ended Linearly Tapered Waveguide Cavities," Tech. Rep. 312436-1, 1988 Electrosci. Lab., Dept. Elec. Eng., Ohio State Univ.

[20]   R. J. Burkholder, "High-Frequency Asymptotic Methods For Analyzing the EM Scattering by Open-Ended Waveguide Cavities," Ph.D. dissertation, 1989, Ohio State University.

[21]   J. J. Boonzaaier and J. A. G. Malherbe, "Electromagnetic Backscatter From Open-Ended Circular Cylinder With Complex Termination," *Electronic Letters,* vol. 23, no. 3, pp. 218-220, Feb. 1989.

[22]   H. Ling, R. Chou, and S. W. Lee, "Shooting and Bouncing Rays: Calculating the RCS of an Arbitrarily Shaped Cavity," *IEEE Trans. Antennas Propagat.,* vol. 37, pp. 194-205, Feb. 1989.

[23]   H. Ling, S. W. Lee, and R. C. Chou, "High-Frequency RCS of Open Cavities with Rectangular and Circular Cross Sections," *IEEE Trans. on Antennas and Propagat.,* vol. 37, no. 5, pp. 648-654, May 1989.

[24]   P. H. Pathak and R. J. Burkholder, "Modal, Ray, and Beam Techniques for Analyzing the EM Scattering by Open-Ended Waveguide Cavities," *IEEE Trans. on Antennas and Propagat.,* vol. 37, no. 5, pp. 635-647, May 1989.

[25]   A. Moghaddar and E. K. Walton, "Time-Frequency Distribution Analysis of Scattering from Waveguide Cavities," *IEEE Trans. on Antennas and Propagat.,* vol. 41, no. 5, pp. 677-680, May 1993.

[26]   H. Kim and H. Ling, "Wavelet Analysis of Radar Echo from Finite-Size Targets," *IEEE Trans. on Antennas and Propagat.,* vol. 41, no. 2, pp. 200-207, Feb. 1993.

[27]   S. Ram and H. Ling, "Application of the Reassigned Joint Time-Frequency Transform to Wideband Scattering From Waveguide Cavities," *IEEE Antennas and Wireless Propagat.*, vol. 6, pp. 580-583, 2007.

[28]   L. N. Medgyesi-Mitschang and J. M. Putnam, "Electromagnetic Scattering from Ducts with Irregular Edges: Part I – Circular Case," *IEEE Trans. on Antennas and Propagat.,* vol. 36 no. 3, pp. 383-397, March 1988.

[29]   *IEEE Recommended Practice for Radar Cross-Section Test Procedures,* IEEE Antennas and Propagation Society, IEEE, N.Y., 2007.

[30]   C. A. Balanis, *Antenna Theory,* John Wiley & Sons, 2005.

[31]   C. A. Balanis, *Advanced Engineering Electromagnetics,* John Wiley & Sons, 1998.

[32]   L. Cohen, *Time-Frequency Analysis,* Prentice-Hall PTR, 1995.

[33]   "Radar Principles," class notes for EE 383v, Department of Electrical and Computer Engineering, University of Texas at Austin, Spring 2009.

[34]   L. C. Trintinalia and H. Ling, "Interpretation of Scattering Phenomenology in Slotted Waveguide Structures via Time-Frequency Processing," *IEEE Trans. Antennas Propagat.,* vol. 43, pp. 1253-1261, Nov. 1995.

[35]   C. S. Lee and S. W. Lee, "RCS of a Coated Circular Waveguide Terminated by a Perfect Conductor," *IEEE Trans. on Antennas and Propagat.,* vol. AP-34, no. 4, pp. 391-398, April 1987.